iScience

CellPress

Article

Conformational Dynamics and Cleavage Sites of Cas12a Are Modulated by Complementarity between crRNA and DNA

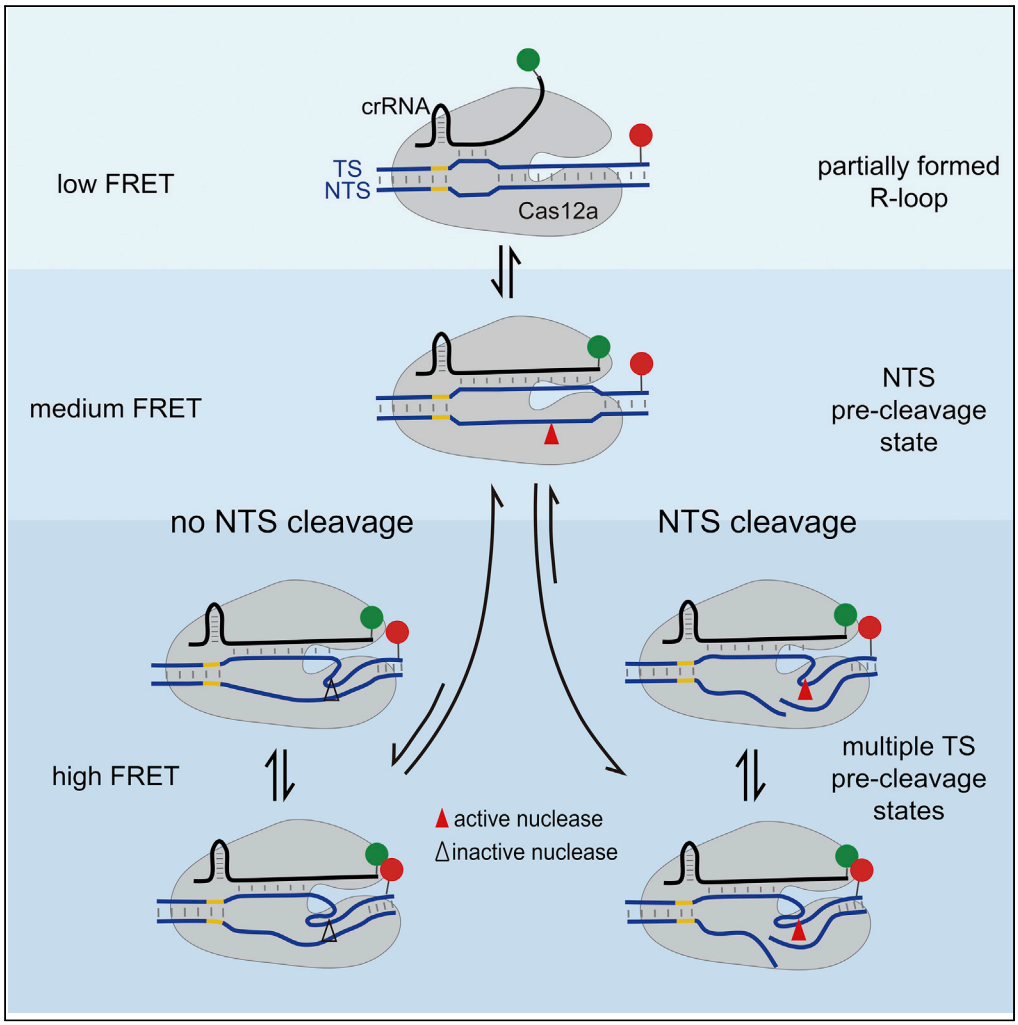

Lujia Zhang, Ruirui Sun, Mengyi Yang, Sijia Peng, Yongxin Cheng, Chunlai Chen

chunlai@mail.tsinghua.edu.cn

HIGHLIGHTS

Dynamic processes of Cas12a contribute to its high specificity

Cleavage sites of non-target strand are released from duplex after DNase activation

Cleaved non-target strand stabilizes target strand pre-cleavage states

Multiple target strand pre-cleavage states target different cleavage sites

Zhang et al., iScience 19, 492–503
September 27, 2019
https://doi.org/10.1016/j.isci.2019.08.005

iScience

CellPress

Article

Conformational Dynamics and Cleavage Sites of Cas12a Are Modulated by Complementarity between crRNA and DNA

Lujia Zhang,[1] Ruirui Sun,[1] Mengyi Yang,[1] Sijia Peng,[1] Yongxin Cheng,[1] and Chunlai Chen[1,2,*]

SUMMARY

Cas12a is an RNA-guided endonuclease, which displays great potentials and several advantages over the well-known Cas9 in genome editing and engineering. Here, we established a quantitative kinetic scheme to describe the conformational dynamics of Cas12a/crRNA/dsDNA ternary complexes. The highly dynamic nature of Cas12a complexes, including their reversible formation, disassembly, and transition between different conformational states, is likely to be one of the key aspects contributing to their high specificity. The non-target strand is cleaved when its cleavage sites are released from DNA duplex after DNase activation of Cas12a. Cleaved non-target strand stabilizes target strand pre-cleavage states to permit subsequent cleavage and to ensure two DNA strands cleaved in a well-defined order. The extent of complementarity between crRNA and DNA modulates the relative stabilities of target strand pre-cleavage states targeting different cleavage sites. Our discoveries provide insights to fully elucidate the working mechanisms of Cas12a and to optimize it for genome engineering.

INTRODUCTION

CRISPR (clustered regularly interspersed short palindromic repeats)-Cas (CRISPR-associated) systems found in bacteria and archaea provide adaptive immunity against exogenous genetic elements (Barrangou et al., 2007; Marraffini and Sontheimer, 2008; Horvath and Barrangou, 2010; Marraffini, 2015). Guide RNAs encoded in CRISPR repeat-spacer arrays are transcribed and processed into individual CRISPR RNAs (crRNAs), which guide Cas proteins to recognize and cleave invading DNAs or RNAs in a sequence-dependent manner (Plagens et al., 2015). Based on the number of Cas proteins in the crRNA-effector complex, CRISPR-Cas systems are divided into two classes. Several Cas proteins are needed to form an effector complex in class I CRISPR-Cas systems, whereas a single multiple-domain Cas protein is sufficient for target recognition and cleavage in class II systems (Makarova et al., 2015; Hille and Charpentier, 2016; Wright et al., 2016). The simplicity of class II CRISPR-Cas systems greatly facilitates their application in genome engineering.

Cas9 protein, especially *Streptococcus pyogenes* Cas9, which belongs to class II type II CRISPR-Cas systems, is most thoroughly investigated and widely used in genome engineering and manipulation (Doudna and Charpentier, 2014; Hsu et al., 2014; Sander and Joung, 2014). Within class II CRISPR-Cas systems, type V Cas12a protein, also known as Cpf1, displays its own unique features and serves as an alternative and complementation to Cas9. *Lachnospiraceae bacterium* Cas12a (LbCas12a) and *Acidaminococcus sp. BV3L6* Cas12a (AsCas12a) exhibited little or no tolerance for mismatches in mammalian gene editing, indicating their higher specificity than Cas9 (Kim et al., 2016; Kleinstiver et al., 2016; Toth et al., 2016; Tu et al., 2017). In addition, Cas12a contains an RNA nuclease domain to process its own precursor crRNA, simplifying its application for multiplexed gene editing (Fonfara et al., 2016; Zetsche et al., 2017). Furthermore, Cas12a exhibits RNA-independent DNase activity and target-binding-induced indiscriminate single-stranded DNase activity, which enable development of novel DNA detection methods with extremely high sensitivity (Sundaresan et al., 2017; Chen et al., 2018; Gootenberg et al., 2018). Therefore, Cas12a has attracted great attention and been widely used (Li et al., 2018; Swarts and Jinek, 2018).

Structural and biochemical studies revealed that Cas12a exhibits a different structural architecture from Cas9, which leads to its distinct molecular mechanisms (Dong et al., 2016; Gao et al., 2016; Yamano et al., 2016, 2017; Stella et al., 2017; Swarts et al., 2017; Jeon et al., 2018; Singh et al., 2018; Strohkendl et al., 2018). Dual tracrRNA:crRNA or a fused single-guide RNA guides Cas9 to recognize 3′ G-rich

[1]School of Life Sciences, Tsinghua-Peking Joint Center for Life Sciences, Beijing Advanced Innovation Center for Structural Biology, Beijing Frontier Research Center for Biological Structure, Tsinghua University, Beijing, China

[2]Lead Contact

*Correspondence: chunlai@mail.tsinghua.edu.cn

https://doi.org/10.1016/j.isci.2019.08.005

protospacer-adjacent motifs (PAMs) on double-stranded DNAs (dsDNAs). Two nuclease domains, HNH and RuvC, are used by Cas9 to cleave dsDNA through their concerted motions to generate blunt ends 3 bp upstream of PAM sites (Jinek et al., 2012; Sternberg et al., 2015). On the other hand, Cas12a is guided by a single crRNA to recognize 5′ T-rich PAMs. Cas12a contains a single RuvC endonuclease domain, which cleaves non-target strand (NTS) and target strand (TS) one by one to create staggered ends (Zetsche et al., 2015; Yamano et al., 2016; Swarts et al., 2017; Jeon et al., 2018; Strohkendl et al., 2018). In addition, evidences showed that Cas12a has multiple cleavage sites on both DNA strands (Stella et al., 2017; Swarts et al., 2017; Strohkendl et al., 2018).

Several single-molecule fluorescence resonance energy transfer (smFRET) assays have been utilized to characterize conformational dynamics of Cas12a (Jeon et al., 2018; Singh et al., 2018; Stella et al., 2018). Singh and coworkers examined how rates of Cas12a/crRNA/dsDNA ternary complex formation and DNA cleavage are modulated by complementarity between crRNA and DNA (Singh et al., 2018). On the other hand, FRET pairs located within *Francisella novicida* Cas12a (FnCas12a) protein and between crRNA and NTS of AsCas12a complexes both showed that Cas12a ternary complexes display several distinctive conformational states, including PAM recognition, R-loop expansion, and NTS and TS pre-cleavage states (Jeon et al., 2018; Stella et al., 2018). Here, using smFRET between crRNA and TS, we established a quantitative kinetic scheme to quantify conformational dynamics of Cas12a ternary complexes and to describe how the extent of crRNA-TS heteroduplex formation modulates transition rates and reaction pathways among different conformational states. We discovered that 14 base pairs of crRNA-DNA heteroduplex at the PAM-proximal end were sufficient to trigger the nuclease activation of Cas12a, whereas more crRNA-DNA base pairs were required to free NTS cleavage sites from DNA duplex to permit cleavage. After NTS cleavage, TS pre-cleavage states were highly stabilized to enable two DNA strands cleaved subsequently. There were several TS pre-cleavage states producing cleaved fragments of different length, whose relative stabilities were modulated by the extent of crRNA-DNA complementarity. Our new findings shed lights on molecular mechanisms of Cas12a-mediated DNA cleavage.

RESULTS

Conformational Dynamics of Cas12a/crRNA/dsDNA Ternary Complexes

To probe the conformational dynamics of Cas12a ternary complexes from their formation until DNA cleavage, we utilized smFRET between crRNA and dsDNA. As shown in Figure 1A, dsDNAs containing Cy5-labeled TS were immobilized on polyethylene glycol-passivated microscope glass slides. An objective-based total internal reflection fluorescence microscope was used to capture smFRET trajectories, whose recording was started 5 s before the delivery of pre-formed Cas12a/crRNA complexes, containing Cy3 at the 3′ end of crRNA (Table S1), to surface immobilized dsDNA (Table S2). Formation of stable Cas12a/crRNA/dsDNA complexes, indicated by black arrows in Figure 1A, caused simultaneous appearance of both Cy3 and Cy5 signals. The increase of Cy3/Cy5 FRET efficiencies evidenced that Cas12a/crRNA/dsDNA complexes underwent a series of conformational changes to bring Cy3- and Cy5-labeling sites close to each other (Figures 1A and 1B). When a full cognate dsDNA containing 23 matched bases toward crRNA was used, termination of FRET signals was accompanied by disappearance of Cy5 signals in ~90% of single-molecule events (blue arrows in Figure 1A). We have carefully adjusted the laser power to obtain optimal signal-to-noise ratio and to minimize the contributions of photobleaching (Figure S1A). Therefore, loss of FRET was due to the release of Cy5-labeled DNA fragments from Cas12a ternary complexes after DNA cleavage (Figures S1B and S1C), which agreed with previous reports (Jeon et al., 2018; Singh et al., 2018; Strohkendl et al., 2018).

We identified four distinctive FRET states from single-molecule trajectories of Cas12a ternary complexes using a Hidden Markov Model-based software (McKinney et al., 2006). They were assigned as S1, S2, S3, and S4 states, whose FRET efficiencies were 0.28 ± 0.01, 0.49 ± 0.01, 0.75 ± 0.01, and 0.95 ± 0.01, respectively. Almost all FRET events were initiated at S1, the lowest FRET state. Interestingly, as shown by representative traces, FRET events could terminate from either S3 or S4 state (Figures 1A and S1C), two highest FRET states, after transiting through an intermediate FRET state (S2). Although the overall trend was that FRET efficiencies of ternary complexes increased over time, spontaneous transitions from a high- to a low-FRET state were commonly detected (Figure 1A). FRET transition density plot (Figure 1C) showed that dynamic transitions mostly occurred between two conformational states whose FRET values were close to each other. Dwell times of each state and transition rates among them were extracted and

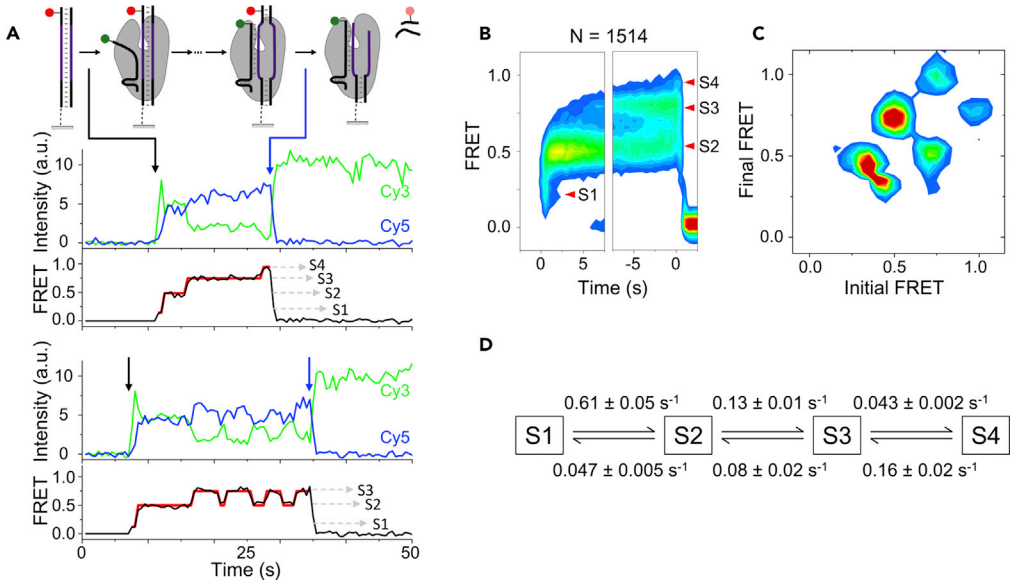

Figure 1. Conformational Dynamics of Cas12a Ternary Complexes on Fully Matched dsDNA

(A) Representative smFRET trajectories and cartoons illustrating corresponding states. Cy3 (green dots) is labeled at 3′ end of crRNA, Cy5 (red dots) is labeled at the TS 28 nucleotides away from the PAM. Black lines are apparent FRET efficiencies, and red lines are hidden Markov modeling of FRET. Immobilized dsDNA contains 23 matched bases toward the crRNA. Under 532 nm excitation, spontaneous appearance of Cy3 and FRET signals represents the formation of Cas12a ternary complexes on immobilized dsDNAs (black arrows), and disappearance of FRET corresponds to dissociation of the cleaved PAM-distal DNA fragments (blue arrows). Four distinctive FRET states are indicated and assigned as S1–S4 from low to high values.

(B) Time-dependent FRET probability density plots synchronized at the appearance of FRET (defined as $t = 0$ in the left panel) or at the disappearance of FRET (defined as $t = 0$ in the right panel). From them, evolution of FRET after complex formation or before release of cleaved DNA can be carefully examined. Overall, FRET efficiencies increase over time after complex formation.

(C) A transition density plot reflecting transition frequencies among FRET states, in which initial and final FRET values for each transition event are accumulated into a two-dimensional histogram.

(D) A kinetic scheme displaying transition pathways and rates (s^{-1}) among different FRET states. All experiments were repeated three times, and SEMs were used as error bars.

quantified. In all, a quantitative kinetic scheme containing four conformational states was established to describe the conformational dynamics of Cas12a ternary complexes (Figure 1D).

Using FRET pairs located on crRNA and NTS, a similar smFRET study by Jeon and colleagues also discovered that AsCas12a ternary complexes present four distinctive FRET states (Jeon et al., 2018). After formation of ternary complexes, AsCas12a gradually transited from the lowest FRET state to the highest FRET state until release of cleaved DNA. Overall, their discoveries and assignment of FRET states are mostly consistent with ours. However, AsCas12a only displays irreversible transitions from low- to high-FRET states and cleaved DNAs are released from the highest FRET state, whereas LbCas12a clearly displays reversible transitions between different conformational states and release of cleaved DNA fragments can occur from either the S3 or S4 state (Figure 1). LbCas12a still displayed similar behaviors when crRNA-NTS FRET pair was used instead of crRNA-TS FRET pair (Figures 1 and S1D). Therefore, we speculated that different Cas12a orthologs could present quite different dynamic and biochemical behaviors originating from their own intrinsic properties (Singh et al., 2018).

Using FRET pairs located on FnCas12a protein, another smFRET study revealed that FnCas12a/crRNA/dsDNA complexes also spontaneously fluctuated among four FRET states. The fact that both LbCas12a and FnCas12a display highly dynamic and reversible transitions among different conformations indicates that they have lower energy barriers among different states than AsCas12a, which might cause LbCas12a and FnCas12a to have faster rates to transit into pre-cleavage states and to cleave dsDNA than AsCas12a (Figure 2) (Singh et al., 2018).

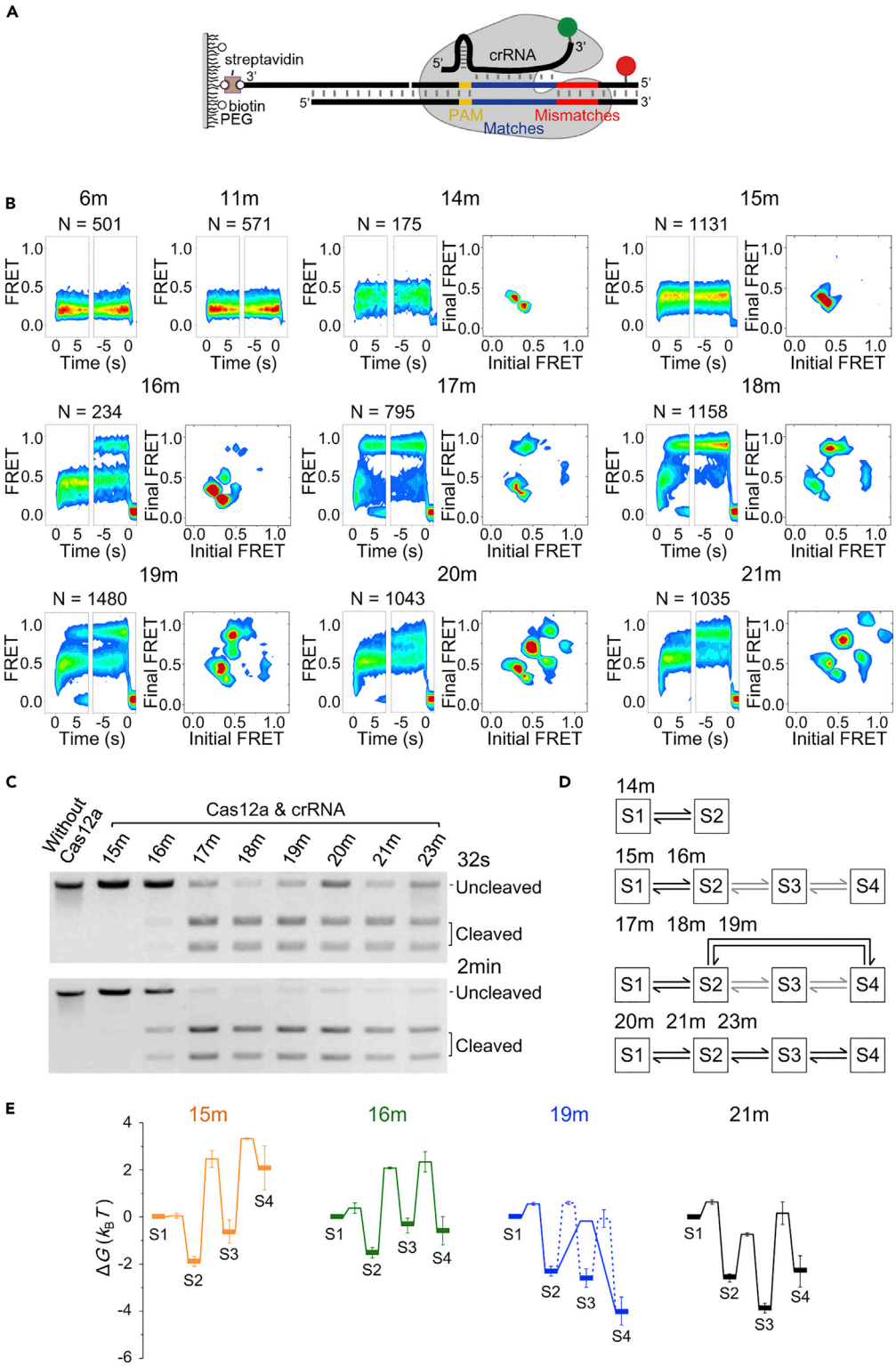

Figure 2. Conformational Dynamics of Cas12a Ternary Complexes on Partial Cognate dsDNAs

(A) Cartoons illustrating immobilization, labeling sites of Cy3 (green dot) and Cy5 (red dot), and positions of crRNA/DNA matches and mismatches.

Figure 2. *Continued*

(B) Time-dependent FRET probability density plots and transition density plots (when applicable) of Cas12a on partial cognate dsDNAs. dsDNAs are named after the number of matched bases between crRNA and TS at their PAM-proximal ends.

(C) Cleavage of dsDNAs by Cas12a at 25°C for 32 s or 2 min.

(D) Kinetic schemes describing dynamics of Cas12a complexes.

(E) Four representative energy landscapes of Cas12a complexes. Bold horizontal lines represent four conformational states captured by smFRET, and thin horizontal lines represent energy barriers along transition pathways. For 19m-dsDNA, which contains parallel reaction pathways, the major pathway is shown in solid lines and the minor pathway in dashed lines. For clarity, energy landscapes of Cas12a with other dsDNAs were displayed in Figure S4C. k_B is the Boltzmann constant and T is the temperature.

Dynamics of Cas12a Complexes on Partial Cognate dsDNAs and Assignment of Conformational States

Using the smFRET assays described above, we quantified how the conformational dynamics of ternary complexes were modulated when partial cognate dsDNA targets were present (Figures 2 and S2). Here, we used the same crRNA and altered the sequence of dsDNA targets, whose names were based on the number of matched bases between crRNA and TS at PAM-proximal end (Figure 2A and Table S2). Therefore, 23m-dsDNA was the cognate target, whereas 6m- and 21m-dsDNAs contained 6 and 21 consecutive matched bases at their PAM-proximal end, respectively.

When 6 or 11 mismatched bases were introduced at the PAM-proximal end of 23m-dsDNA, almost no Cas12a/crRNA-binding events or FRET signals were detected. On the other hand, Cas12a complexes containing 6 and 11 matched bases at the PAM-proximal end both exhibited a single FRET state corresponding to the S1 state (Figures 2B and S2). In addition, disappearance of their FRET signals was caused by dissociation of Cy3-labeled Cas12a/crRNA from immobilized dsDNA, because FRET and Cy3 signals disappeared simultaneously in most cases (~90%, example traces shown in Figure S2). Thus, S1 is an intermediate state formed after PAM recognition and partial R-loop formation.

The S2 state appeared when there were 14 matched bases between crRNA and TS at the PAM-proximal end. Under such condition, Cas12a complexes mainly fluctuated between the S1 and S2 states and barely sampled the S3 or S4 states (Figures 2B and S2). The populations of S3 and S4 increased to 9% $\pm$ 1% and 11% $\pm$ 4%, respectively, when 16m-dsDNA was used. With dsDNAs containing 17 or more matched bases toward crRNA, Cas12a complexes quickly transited through the low-FRET S1 and S2 states and mainly stayed in one of the high-FRET states, S3 or S4. Their abilities to quickly transit into S3 or S4 strongly correlated with their cleavage activities (Figures 2B and 2C). In addition, dissociation of cleaved DNA fragments, indicated by disappearance of FRET and Cy5 signals, can also occur from either S3 or S4 (Figures 1A, S1C, and S2). These results suggested that S3 and S4 states are likely to fulfill similar functions. Previous results from single-molecule and ensemble biochemical measurements suggested that the cleavage of NTS precedes the cleavage of TS (Jeon et al., 2018; Stella et al., 2018; Strohkendl et al., 2018). Using Cy3-labeled NTS and Cy5-labeled TS, we also discovered that cleaved NTS fragments were released before cleaved TS in most cases (Figure S3). Together, we proposed that S2 is the NTS pre-cleavage state formed when the R-loop is extended to the PAM-distal end. Both S3 and S4 represent TS pre-cleavage states, whose difference will be described below.

Energy Landscapes of Cas12a Complexes

Cas12a complexes containing 14 or more matched bases between crRNA and TS displayed transitions among different conformational states (Figures 2B and 2D). Based on their major transition pathways, quantitative kinetic schemes containing transition rates extracted from single-molecule trajectories were established (Figures S4A and S4B). The differences in free energies between conformational states and the energy barriers along reaction pathways were quantified and used to plot energy landscapes of Cas12a complexes with partial cognate and full cognate dsDNAs (Figures 2E and S4C).

Several features of conformational dynamics of Cas12a complexes could be summarized from their FRET patterns and energy landscapes. (1) Once Cas12a ternary complexes were formed, they were initiated at the S1 state, an intermediate state containing partially formed R-loop. In our experiments, Cas12a complexes remained in S1 when matched bases between crRNA and TS were 11 or less, whereas Cas12a could advance to other states when matched bases were 14 or more. (2) When dsDNA contained 14 or more

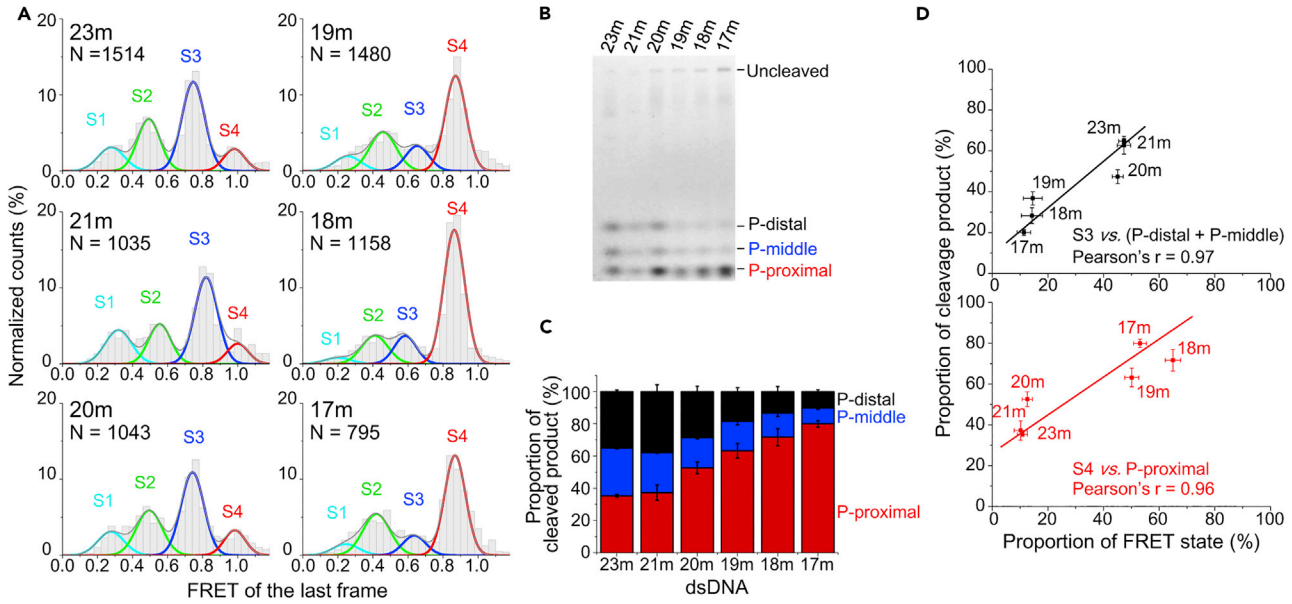

Figure 3. Correlation between FRET Pattern and TS Cleavage Pattern of Cas12a

(A) FRET distributions of Cas12a complexes in the last frame before disappearance of FRET.

(B) Cleavage of TS. dsDNAs are labeled at the PAM-distal end of TSs. Three cleaved fragments of different lengths are separated on 15% urea-PAGE. They are assigned as P-distal, P-middle, and P-proximal, whose cleavage sites on TS are about +26, +25, and +24, respectively (Figure S5B).

(C) Proportion of cleaved TS fragments of different lengths.

(D) Linear correlation between proportion of FRET states and proportion of TS fragments. They display a strong positive correlation with Pearson's $r \geq 0.96$.

All experiments were repeated three times, and SEMs were used as error bars.

matched bases toward crRNA, transition rates from S1 to S2 were fast (0.48–1.00 s^{-1}, Figure S4B). However, biochemical assays revealed that 14m-dsDNA could not be cleaved and cleavage of 15m-dsDNA and 16m-dsDNA required several minutes or more (Figures 2C and S5A) (Stella et al., 2018). These results suggested that Cas12a complexes containing intact dsDNAs are able to quickly access S2, the NTS pre-cleavage state, from the initial S1 state after further extension of the R-loop. (3) The S3 state was the most stable state when there were 20 or more matched bases between crRNA and TS. On the other hand, the S4 state became the most stable state and Cas12a displayed significant transition from S2 to S4 when there were 17–19 matched bases. Our observation that dsDNAs containing 17–23 matches were all cleaved by Cas12a at similar rates supports our assignment that both S3 and S4 are TS pre-cleavage states (Figure 2C). In the presence of 15 or 16 matched bases, cleavage rate was significantly slower because S3 and S4 became less stable than S2 and were sampled by Cas12a complexes at low frequencies (Figures 2B and 2E).

S3 and S4 States Are TS Pre-cleavage States Targeting Different Cleavage Sites

Recent reports (Stella et al., 2017; Swarts et al., 2017; Strohkendl et al., 2018) indicated that Cas12a could cleave TS at different sites and produce fragments with different lengths. We hypothesized that the S3 and S4 states target different cleavage sites. The proportion of Cas12a complexes staying in S4 as the last state before disappearance of FRET increased from 11% ± 2% with 23m-dsDNA to 53% ± 2% with 17m-dsDNA (Figure 3A). Using Cy5-labeled TS, we discovered that there were three cleaved TS fragments of different lengths (Figures 3B and S5B). The proportion of cleaved product P-proximal increased from 35% ± 1% with 23m-dsDNA to 80% ± 2% with 17m-dsDNA (Figure 3C). Thus the proportion of the S4 FRET state strongly correlated with the proportion of cleaved product P-proximal, whereas the proportion of the S3 FRET state strongly correlated with the proportion of cleaved products P-distal and P-middle (Figure 3D). Together, our results supported the model that both S3 and S4 states are pre-cleavage states targeting different TS cleavage sites to produce fragments of different lengths.

NTS Cleavage Site Is Freed from DNA Duplex after DNase Activation of Cas12a

Although Cas12a displayed no cleavage activities toward 14m-dsDNA within 30 min (Figure S5A), the TS of 14m-dsDNA in its single-stranded form was able to induce indiscriminate single-stranded DNase activity of

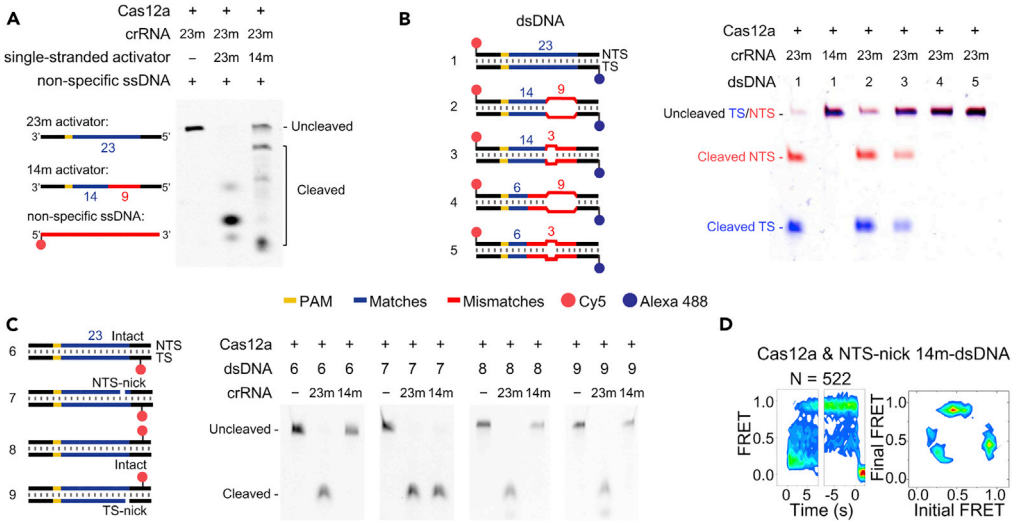

Figure 4. Cleavage and smFRET of Pre-unwound or Pre-cleaved DNAs

(A) Indiscriminate single-stranded DNA cleavage activated by 23m- or 14m- single-stranded activators, which contain 23 and 14 matched bases toward 23m-crRNA at the PAM-proximal end, respectively. Matched bases toward 23m-crRNA are shown in blue, whereas mismatched bases toward 23m-crRNA are shown in red. Non-specific ssDNA was labeled with Cy5 at the 5′ end.

(B) Cleavage of pre-unwound dsDNAs. Cas12a was guided by 23m-crRNA or 14m-crRNA, which contain 23 or 14 matched bases at their PAM-proximal ends toward 23m-dsDNA, respectively. Pre-unwound segments are plotted as bulges. Labeling sites are shown in cartoons.

(C) Cleavage of 23m-dsDNA containing pre-cleaved NTS or TS. Locations of the pre-cleaved and labeling sites are shown in cartoons. In the presence of 14m-crRNA, pre-cleaved NTS (NTS-nick) caused cleavage of TS (dsDNA #7), whereas pre-cleaved TS (TS-nick) did not lead to cleavage of NTS (dsDNA #9).

(D) Time-dependent FRET probability density and transition density plots of Cas12a complexes on NTS-nick 14m-dsDNAs.

Cas12a (Figure 4A). In addition, pre-unwound 14m-dsDNAs containing mismatches between TS and NTS from +15 to +17 or from +15 to +23 can be cleaved by Cas12a, whereas pre-unwound 6m-dsDNAs containing mismatches at the same sites cannot be cleaved (Figure 4B). Together, these results suggested that 14 base pairs between crRNA and TS at the PAM-proximal end were sufficient to trigger the nuclease activation of Cas12a. The NTS cleavage site located around +18 is freed in pre-unwound dsDNAs to permit its accessibility and cleavage, whereas the NTS cleavage site in 14m-dsDNA remains in its duplex form and thus prevents further cleavage. Therefore, we speculated that freeing single-stranded NTS from DNA duplex is an important checkpoint after nuclease activation and 17 or more base pairs between crRNA and TS are needed to fully release NTS cleavage site to enable quick cleavage (Figure 2C).

NTS Cleavage Governs TS Cleavage

Next, we introduced nicks at the cleavage sites of the NTS (termed NTS-nick) or the TS (termed TS-nick) to generate dsDNAs containing pre-cleaved NTS or pre-cleaved TS. When there were only 14 matched bases between crRNA and TS at the PAM-proximal end, pre-cleaved NTS led to significant cleavage of TS, whereas no cleavage of NTS was detected in the presence of pre-cleaved TS (Figure 4C). smFRET measurements also showed that Cas12a with NTS-nick 14m-dsDNA can quickly transit to TS pre-cleavage states (Figure 4D), whereas Cas12a with intact 14m-dsDNA barely samples TS pre-cleavage states (Figure 2B). Together, our observation that pre-cleaved NTS permitted cleavage of TS and cleavage of NTS was not affected by pre-cleaved TS suggested that NTS cleavage precedes and governs TS cleavage.

TS Pre-cleavage States Are Stabilized after NTS Cleavage

To examine how cleavage of NTS affects the dynamics of Cas12a complexes, we used dCas12a whose nuclease activity is completely abolished by introducing the E925A point mutation (Yamano et al., 2017). Interestingly, dCas12a ternary complexes formed with intact 23m-dsDNA also displayed all four FRET states as we described above (Figure 5A). However, dCas12a complexes mainly stayed in the NTS

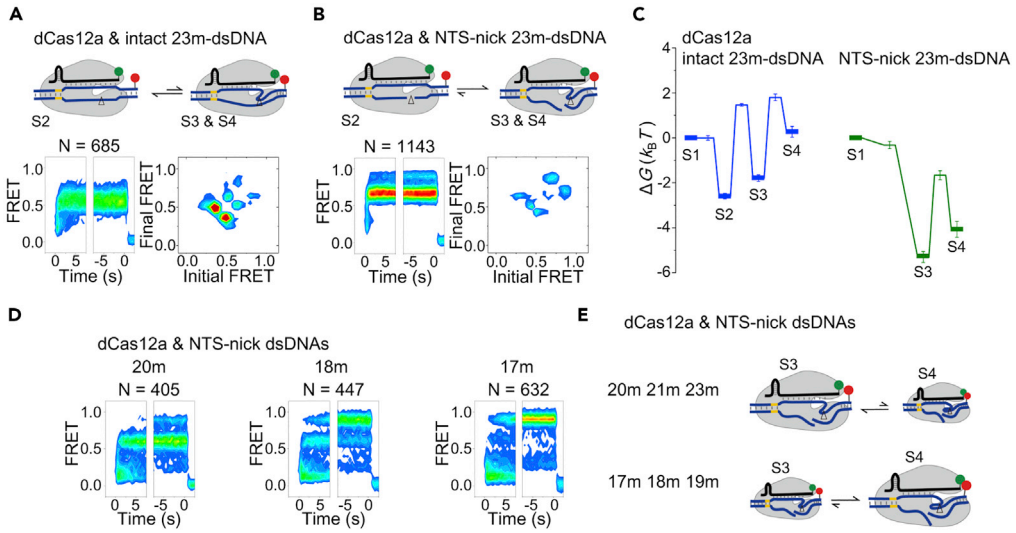

Figure 5. Conformational Dynamics of dCas12a Complexes

(A and B) Time-dependent FRET probability density plots and transition density plots of dCas12a complexes on intact (A) or NTS-nick (B) 23m-dsDNAs.

(C) Energy landscapes of dCas12a complexes on intact or NTS-nick 23m-dsDNAs.

(D) Time-dependent FRET probability density plots of dCas12a complexes on NTS-nick 20m-, 18m-, and 17m-dsDNAs.

(E) Cartoons demonstrating how transition rates between TS-pre-cleavage states S3 and S4 were modulated by the extent of crRNA-DNA complementarity.

pre-cleavage state (S2 state) and occasionally sampled the TS pre-cleavage states (S3 and S4 states, Figures 5A and S6). From energy landscape, we can clearly visualize that S3 and S4 were less stable than S2 for dCas12a (Figure 5C), whereas S3 and S4 were stabilized and at least one of them became more stable than S2 for active Cas12a complexes (Figures 2E and S4C). With dsDNA containing pre-cleaved NTS (NTS-nick), dCas12a complexes quickly transited into and mainly stayed in the TS pre-cleavage states, S3 and S4 (Figures 5B and S6). We quantified that the presence of pre-cleaved NTS in dCas12a/23m-dsDNA complexes stabilized the S3 and S4 states ($\Delta G = -3.5 \pm 0.3$ and -4.4 ± 0.4 k_BT, respectively) and destabilized the S2 state ($\Delta G = 1.2 \pm 0.3$ k_BT) (Figure 5C). Together, our results suggested that Cas12a complexes containing intact NTS can only transiently sample TS pre-cleavage states, whereas cleaved NTS stabilized TS pre-cleavage states to facilitate subsequent cleavage step.

When pre-cleaved NTS was introduced into 20m-, 18m-, and 17m-dsDNAs, proportion of S4 increased when the number of matched bases decreased (Figures 5D and 5E). Similar behaviors were also captured using Cas12a complexes (Figures 2B and 3A). These results indicated that the relative stabilities of TS pre-cleavage states, S3 and S4, were modulated by the extent of complementarity between crRNA and TS.

DISCUSSION

Previous structural and biochemical studies (Stella et al., 2017, 2018; Jeon et al., 2018; Strohkendl et al., 2018) indicated that Cas12a ternary complexes went through a highly dynamic process to permit dsDNA cleavage, whose main steps included crRNA invasion, R-loop formation, R-loop expansion, and conformational changes to allow two DNA strands to be cleaved by the RuvC nuclease domain sequentially. Here, we utilized FRET pair located on the crRNA and TS to capture the conformational dynamics of individual Cas12a complexes from their formation until release of cleaved DNA fragments in detail. Four distinctive conformational states distinguished by their FRET efficiencies were identified by our smFRET measurements. In addition to previous discoveries, we established the following quantitative kinetic scheme to describe the reaction pathways of Cas12a ternary complexes (Figure 6). When the Cas12a/crRNA binary complex recognizes its target, ternary complex is formed in the S1 FRET state, an intermediate state containing partially formed R-loop. Extension of the R-loop to the PAM-distal end causes further interactions between Cas12a and the heteroduplex, which trigger conformational changes of Cas12a to activate its nuclease center and to adopt the NTS pre-cleavage conformational state identified as the S2 FRET state.

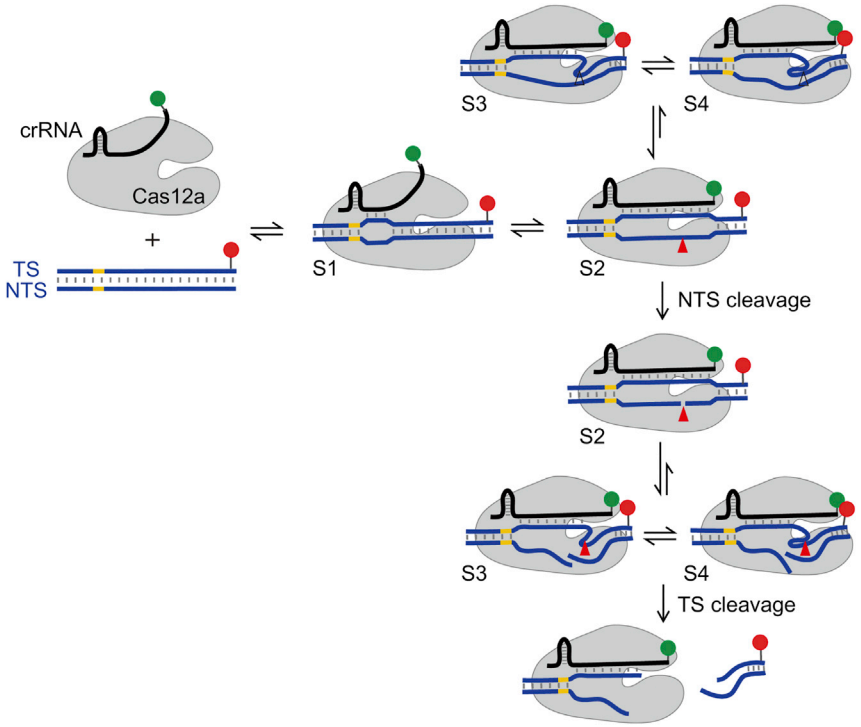

Figure 6. A Kinetic Scheme Describing Reaction Pathways of Cas12a/crRNA/dsDNA Ternary Complexes from Formation Until DNA Cleavage

Cas12a proteins are shown in gray, crRNAs are shown in black, and dsDNAs are shown in purple. Cy3 and Cy5 are labeled at crRNAs and TSs of dsDNAs, respectively. Two-way and one-way arrows indicate reversible and irreversible reactions, respectively. Once Cas12a/crRNA binary complexes recognize their target sites and initiate the R-loop formation, ternary complexes are formed in the S1 state. Cas12a complexes transit into the S2 state when the R-loop is extended to contain 14 or more base pairs. Cas12a complexes containing intact NTS can only transiently sample S3 and S4 states from S2 without carrying out TS cleavage. After irreversible cleavage of NTS, S3 and S4 states are stabilized, in which the nuclease activation centers target different cleavage sites on TS. Cleavage of TS occurring from S3 and S4 generates cleaved TS fragments of different lengths, and PAM-distal fragments are released from the complexes.

Cas12a complex containing intact NTS can only transiently sample S3 and S4 states, TS pre-cleavage states targeting different cleavage sites. Once NTS is cleaved, TS pre-cleavage states are greatly stabilized and become long-lived states. The extent of complementarity between crRNA and TS modulates the relative stabilities of S3 and S4, which eventually causes different patterns of cleaved TS fragments (Figure 3B). Last, the PAM-distal DNA fragments quickly dissociate from the complexes, whereas the PAM-proximal DNA fragments remain bound with Cas12a/crRNA.

Previous studies showed that the length and composition of the 5′ end of crRNA affected the nuclease activities of Cas12a (Park et al., 2018; Singh et al., 2018). Here, we used a crRNA, which contained four G nucleotides at its 5′ end and displayed slower cleavage rate than the crRNA containing a single U at its 5′ end, to repeat several experiments described above (Figure S7). In general, stabilities of different conformational states and transition rates among them were moderately affected by G nucleotides at the 5′ end of the crRNA, whereas the overall reaction pathways and kinetic schemes remained the same.

Unlike Cas9, which can form stable binding on off-target sites containing eight or more base pairs at the PAM-proximal end without cleaving dsDNA (Singh et al., 2016), Cas12a has to cleave dsDNA to remain stably bound (Singh et al., 2018). Our kinetic scheme provides an explanation toward such phenomena (Figure 6). Cas12a complexes containing intact dsDNAs could disassemble quickly through a series of reversible steps, whereas irreversible cleavage steps of DNA prevent disassembly process. Furthermore, in the presence of partial cognate dsDNA targets containing 15 or 16 matched bases, competition between the disassembly and cleavage steps causes a lot of unproductive formation of Cas12a ternary complexes

(Jeon et al., 2018; Singh et al., 2018), which reduces effective cleavage rates sharply (Figures 2C and S5A). Similarly, the ribosome utilizes a series of reversible steps to compete with forward reactions to achieve high specificity in tRNA selection (Pape et al., 1998; Geggier et al., 2010). Therefore the highly dynamic nature of Cas12a ternary complexes is likely to be one of the key mechanisms contributing to their higher specificity than Cas9 (Kim et al., 2016; Kleinstiver et al., 2016; Toth et al., 2016; Tu et al., 2017).

Conformational changes of Cas12a protein, including movements of the REC linker, lid, and finger to interact with heteroduplex at several locations, serve as the checkpoints to activate its nuclease catalytic center (Stella et al., 2018). Here, we discovered that 14 matched bases between crRNA and TS at the PAM-proximal end are sufficient to trigger nuclease activation of Cas12a, including its indiscriminate nuclease activity (Figures 4A–4C). Our observation, that Cas12a cannot cleave intact 14m-dsDNA but can cleave 14m-dsDNA containing pre-cleaved NTS or pre-unwound NTS, indicated that 14 base pairs between crRNA and TS are insufficient to release NTS cleavage sites (around +18) from dsDNA. On the other hand, in the presence of 17 or more base pairs between crRNA and TS or pre-unwound dsDNA targets, NTS cleavage sites are fully released. Therefore, NTS cleavage and subsequent TS cleavage are carried out quickly once the nuclease center is activated (Figure 2C). Together, we proposed that, after Cas12a nuclease activation, the R-loop has to extend further to free NTS cleavage sites from the DNA duplex, which is another important checkpoint to permit its accessibility and cleavage.

Although dCas12a complexes containing intact 23m-dsDNA can transiently sample TS pre-cleavage states S3 and S4, they are less stable than S3 and S4 states of active Cas12a or dCas12a containing pre-cleaved NTS (Figures 5C and S4C). In addition, FRET efficiencies of S3 and S4 states of dCas12a (0.65 $\pm$ 0.04 and 0.89 $\pm$ 0.03 for intact 23m-dsDNA) were significantly smaller than the corresponding values of Cas12a (0.75 $\pm$ 0.01 and 0.95 $\pm$ 0.01), which indicated that their conformational structures are similar but not exactly the same. Thus the presence of intact NTS protects TS from cleavage by destabilizing TS pre-cleavage states and preventing the correct positioning of Cas12a catalytic center toward cleavage sites on TS. Once NTS is cleaved, TS pre-cleavage states are stabilized in the correct conformations to license subsequent cleavage of TS. As a result, two DNA strands are cleaved in a sequentially coordinated fashion.

Until now, there is no direct structural information regarding how Cas12a cuts its TS. It is proposed that Cas12a and Cas12b may utilize similar mechanisms to cleave TS. In structures of AacCas12b complexes, TS adopts a sharp bending to bind the RuvC catalytic center in the same polarity as NTS does (Yang et al., 2016). To achieve such conformation after NTS cleavage, additional conformational rearrangements of Cas12a complexes in combination with shortening the crRNA-TS heteroduplex are required to correctly target TS cleavage sites (Stella et al., 2018). Here, we proposed that TS pre-cleavage states, S3 and S4, contain different bending conformations of TS caused by different extent of heteroduplex unwinding. According to our proposed model (Figure 6), Cas12a complexes with more PAM-distal-end mismatches are more likely to further unwind the R-loop, to cause further bending of TS, and to cleave at sites closer to the PAM, than the ones containing fewer or no mismatches. Such speculation is fully consistent with our observation (Figures 3 and S7). Overall, our smFRET measurements provided direct evidences that Cas12a complexes can access multiple conformations in their TS pre-cleavage states.

Based on our established kinetic scheme, we speculated that one of the key aspects leading to high specificity of Cas12a is the reversible formation of Cas12a/crRNA/dsDNA complexes before DNA cleavage, which reduces effective cleavage rates toward off-target DNAs sharply. Release of NTS cleavage sites from DNA duplex serves as another important checkpoint after nuclease activation to initiate cleavage steps. NTS cleavage precedes and licenses TS cleavage to ensure that Cas12a cleaves both DNA strands in a well-ordered coordinated fashion. Cas12a complexes in TS pre-cleavage states adopt several alternative conformations targeting and cleaving different sites on TS. Thus, our findings provide insights to elucidate the working mechanisms of Cas12a and to optimize and engineer Cas12a as an effective and multipurpose tool in genome editing and manipulation.

Limitations of the Study

We do want to point out that LbCas12a generates three cleaved TS fragments of different lengths, which indicates that there should be three TS pre-cleavage conformational states targeting different sites. However, different conformational states might present similar FRET efficiencies and be assigned as a single

FRET state, when their differences cannot be resolved by the distance between FRET-labeling sites (Stella et al., 2018). As a result, we only captured two FRET states, S3 and S4, as TS pre-cleavage states.

METHODS

All methods can be found in the accompanying Transparent Methods supplemental file.

SUPPLEMENTAL INFORMATION

Supplemental Information can be found online at https://doi.org/10.1016/j.isci.2019.08.005.

ACKNOWLEDGMENTS

This project was supported by funds from the National Natural Science Foundation of China (21877069 and 31570754), Tsinghua-Peking Joint Center for Life Sciences, Beijing Advanced Innovation Center for Structural Biology, and Beijing Frontier Research Center for Biological Structure to C.C. The authors would like to thank Dr. Zhiwei Huang from Harbin Institute of Technology for providing plasmid to express LbCas12a.

AUTHOR CONTRIBUTIONS

L.Z. and C.C. designed the experiments; L.Z., R.S., M.Y., S.P., and Y.C. prepared materials and reagents; L.Z. and R.S. performed experiments; L.Z. and C.C. analyzed the data and wrote the paper.

DECLARATION OF INTERESTS

The authors declare no competing interests.

Received: May 4, 2019
Revised: July 15, 2019
Accepted: August 2, 2019
Published: September 27, 2019

REFERENCES

Barrangou, R., Fremaux, C., Deveau, H., Richards, M., Boyaval, P., Moineau, S., Romero, D.A., and Horvath, P. (2007). CRISPR provides acquired resistance against viruses in prokaryotes. Science *315*, 1709–1712.

Chen, J.S., Ma, E., Harrington, L.B., Da Costa, M., Tian, X., Palefsky, J.M., and Doudna, J.A. (2018). CRISPR-Cas12a target binding unleashes indiscriminate single-stranded DNase activity. Science *360*, 436–439.

Dong, D., Ren, K., Qiu, X., Zheng, J., Guo, M., Guan, X., Liu, H., Li, N., Zhang, B., Yang, D., et al. (2016). The crystal structure of Cpf1 in complex with CRISPR RNA. Nature *532*, 522–526.

Doudna, J.A., and Charpentier, E. (2014). Genome editing. The new frontier of genome engineering with CRISPR-Cas9. Science *346*, 1258096.

Fonfara, I., Richter, H., Bratovic, M., Le Rhun, A., and Charpentier, E. (2016). The CRISPR-associated DNA-cleaving enzyme Cpf1 also processes precursor CRISPR RNA. Nature *532*, 517–521.

Gao, P., Yang, H., Rajashankar, K.R., Huang, Z., and Patel, D.J. (2016). Type V CRISPR-Cas Cpf1 endonuclease employs a unique mechanism for crRNA-mediated target DNA recognition. Cell Res. *26*, 901–913.

Geggier, P., Dave, R., Feldman, M.B., Terry, D.S., Altman, R.B., Munro, J.B., and Blanchard, S.C. (2010). Conformational sampling of aminoacyl-tRNA during selection on the bacterial ribosome. J. Mol. Biol. *399*, 576–595.

Gootenberg, J.S., Abudayyeh, O.O., Kellner, M.J., Joung, J., Collins, J.J., and Zhang, F. (2018). Multiplexed and portable nucleic acid detection platform with Cas13, Cas12a, and Csm6. Science *360*, 439–444.

Hille, F., and Charpentier, E. (2016). CRISPR-Cas: biology, mechanisms and relevance. Philos. Trans. R. Soc. Lond. B Biol. Sci. *371*, https://doi.org/10.1098/rstb.2015.0496.

Horvath, P., and Barrangou, R. (2010). CRISPR/Cas, the immune system of bacteria and archaea. Science *327*, 167–170.

Hsu, P.D., Lander, E.S., and Zhang, F. (2014). Development and applications of CRISPR-Cas9 for genome engineering. Cell *157*, 1262–1278.

Jeon, Y., Choi, Y.H., Jang, Y., Yu, J., Goo, J., Lee, G., Jeong, Y.K., Lee, S.H., Kim, I.S., Kim, J.S., et al. (2018). Direct observation of DNA target searching and cleavage by CRISPR-Cas12a. Nat. Commun. *9*, 2777.

Jinek, M., Chylinski, K., Fonfara, I., Hauer, M., Doudna, J.A., and Charpentier, E. (2012). A programmable dual-RNA-guided DNA endonuclease in adaptive bacterial immunity. Science *337*, 816–821.

Kim, D., Kim, J., Hur, J.K., Been, K.W., Yoon, S.H., and Kim, J.S. (2016). Genome-wide analysis reveals specificities of Cpf1 endonucleases in human cells. Nat. Biotechnol. *34*, 863–868.

Kleinstiver, B.P., Tsai, S.Q., Prew, M.S., Nguyen, N.T., Welch, M.M., Lopez, J.M., McCaw, Z.R., Aryee, M.J., and Joung, J.K. (2016). Genome-wide specificities of CRISPR-Cas Cpf1 nucleases in human cells. Nat. Biotechnol. *34*, 869–874.

Li, T., Zhu, L., Xiao, B., Gong, Z., Liao, Q., and Guo, J. (2018). CRISPR-Cpf1-mediated genome editing and gene regulation in human cells. Biotechnol. Adv. https://doi.org/10.1016/j.biotechadv.2018.10.013.

Makarova, K.S., Wolf, Y.I., Alkhnbashi, O.S., Costa, F., Shah, S.A., Saunders, S.J., Barrangou, R., Brouns, S.J., Charpentier, E., Haft, D.H., et al. (2015). An updated evolutionary classification of CRISPR-Cas systems. Nat. Rev. Microbiol. *13*, 722–736.

Marraffini, L.A. (2015). CRISPR-Cas immunity in prokaryotes. Nature *526*, 55.

Marraffini, L.A., and Sontheimer, E.J. (2008). CRISPR interference limits horizontal gene transfer in staphylococci by targeting DNA. Science *322*, 1843–1845.

McKinney, S.A., Joo, C., and Ha, T. (2006). Analysis of single-molecule FRET trajectories using hidden Markov modeling. Biophys. J. *91*, 1941–1951.

Pape, T., Wintermeyer, W., and Rodnina, M.V. (1998). Complete kinetic mechanism of elongation factor Tu-dependent binding of aminoacyl-tRNA to the A site of the E. coli ribosome. EMBO J. *17*, 7490–7497.

Park, H.M., Liu, H., Wu, J., Chong, A., Mackley, V., Fellmann, C., Rao, A., Jiang, F., Chu, H., Murthy, N., et al. (2018). Extension of the crRNA enhances Cpf1 gene editing in vitro and in vivo. Nat. Commun. *9*, 3313.

Plagens, A., Richter, H., Charpentier, E., and Randau, L. (2015). DNA and RNA interference mechanisms by CRISPR-Cas surveillance complexes. FEMS Microbiol. Rev. *39*, 442–463.

Sander, J.D., and Joung, J.K. (2014). CRISPR-Cas systems for editing, regulating and targeting genomes. Nat. Biotechnol. *32*, 347–355.

Singh, D., Mallon, J., Poddar, A., Wang, Y., Tippana, R., Yang, O., Bailey, S., and Ha, T. (2018). Real-time observation of DNA target interrogation and product release by the RNA-guided endonuclease CRISPR Cpf1 (Cas12a). Proc. Natl. Acad. Sci. U S A *115*, 5444–5449.

Singh, D., Sternberg, S.H., Fei, J., Doudna, J.A., and Ha, T. (2016). Real-time observation of DNA recognition and rejection by the RNA-guided endonuclease Cas9. Nat. Commun. *7*, 12778.

Stella, S., Alcon, P., and Montoya, G. (2017). Structure of the Cpf1 endonuclease R-loop complex after target DNA cleavage. Nature *546*, 559–563.

Stella, S., Mesa, P., Thomsen, J., Paul, B., Alcón, P., Jensen, S.B., Saligram, B., Moses, M.E., Hatzakis, N.S., and Montoya, G. (2018). Conformational activation promotes CRISPR-Cas12a catalysis and resetting of the endonuclease activity. Cell *175*, 1856–1871.e21.

Sternberg, S.H., LaFrance, B., Kaplan, M., and Doudna, J.A. (2015). Conformational control of DNA target cleavage by CRISPR-Cas9. Nature *527*, 110–113.

Strohkendl, I., Saifuddin, F.A., Rybarski, J.R., Finkelstein, I.J., and Russell, R. (2018). Kinetic basis for DNA target specificity of CRISPR-Cas12a. Mol. Cell *71*, 816–824.e3.

Sundaresan, R., Parameshwaran, H.P., Yogesha, S.D., Keilbarth, M.W., and Rajan, R. (2017). RNA-independent DNA cleavage activities of Cas9 and Cas12a. Cell Rep. *21*, 3728–3739.

Swarts, D.C., and Jinek, M. (2018). Cas9 versus Cas12a/Cpf1: structure-function comparisons and implications for genome editing. Wiley Interdiscip. Rev. RNA, e1481, https://doi.org/10.1002/wrna.1481.

Swarts, D.C., van der Oost, J., and Jinek, M. (2017). Structural basis for guide RNA processing and seed-dependent DNA targeting by CRISPR-Cas12a. Mol. Cell *66*, 221–233.e4.

Toth, E., Weinhardt, N., Bencsura, P., Huszar, K., Kulcsar, P.I., Talas, A., Fodor, E., and Welker, E. (2016). Cpf1 nucleases demonstrate robust activity to induce DNA modification by exploiting homology directed repair pathways in mammalian cells. Biol. Direct *11*, 46.

Tu, M., Lin, L., Cheng, Y., He, X., Sun, H., Xie, H., Fu, J., Liu, C., Li, J., Chen, D., et al. (2017). A 'new lease of life': FnCpf1 possesses DNA cleavage activity for genome editing in human cells. Nucleic Acids Res. *45*, 11295–11304.

Wright, A.V., Nunez, J.K., and Doudna, J.A. (2016). Biology and applications of CRISPR systems: harnessing nature's toolbox for genome engineering. Cell *164*, 29–44.

Yamano, T., Nishimasu, H., Zetsche, B., Hirano, H., Slaymaker, I.M., Li, Y., Fedorova, I., Nakane, T., Makarova, K.S., Koonin, E.V., et al. (2016). Crystal structure of Cpf1 in complex with guide RNA and target DNA. Cell *165*, 949–962.

Yamano, T., Zetsche, B., Ishitani, R., Zhang, F., Nishimasu, H., and Nureki, O. (2017). Structural basis for the canonical and non-canonical PAM recognition by CRISPR-Cpf1. Mol. Cell *67*, 633–645.e3.

Yang, H., Gao, P., Rajashankar, K.R., and Patel, D.J. (2016). PAM-dependent target DNA recognition and cleavage by C2c1 CRISPR-Cas endonuclease. Cell *167*, 1814–1828.e12.

Zetsche, B., Gootenberg, J.S., Abudayyeh, O.O., Slaymaker, I.M., Makarova, K.S., Essletzbichler, P., Volz, S.E., Joung, J., van der Oost, J., Regev, A., et al. (2015). Cpf1 is a single RNA-guided endonuclease of a class 2 CRISPR-Cas system. Cell *163*, 759–771.

Zetsche, B., Heidenreich, M., Mohanraju, P., Fedorova, I., Kneppers, J., DeGennaro, E.M., Winblad, N., Choudhury, S.R., Abudayyeh, O.O., Gootenberg, J.S., et al. (2017). Multiplex gene editing by CRISPR-Cpf1 using a single crRNA array. Nat. Biotechnol. *35*, 31–34.

ISCI, Volume *19*

Supplemental Information

Conformational Dynamics and Cleavage Sites of Cas12a Are Modulated by Complementarity between crRNA and DNA

Lujia Zhang, Ruirui Sun, Mengyi Yang, Sijia Peng, Yongxin Cheng, and Chunlai Chen

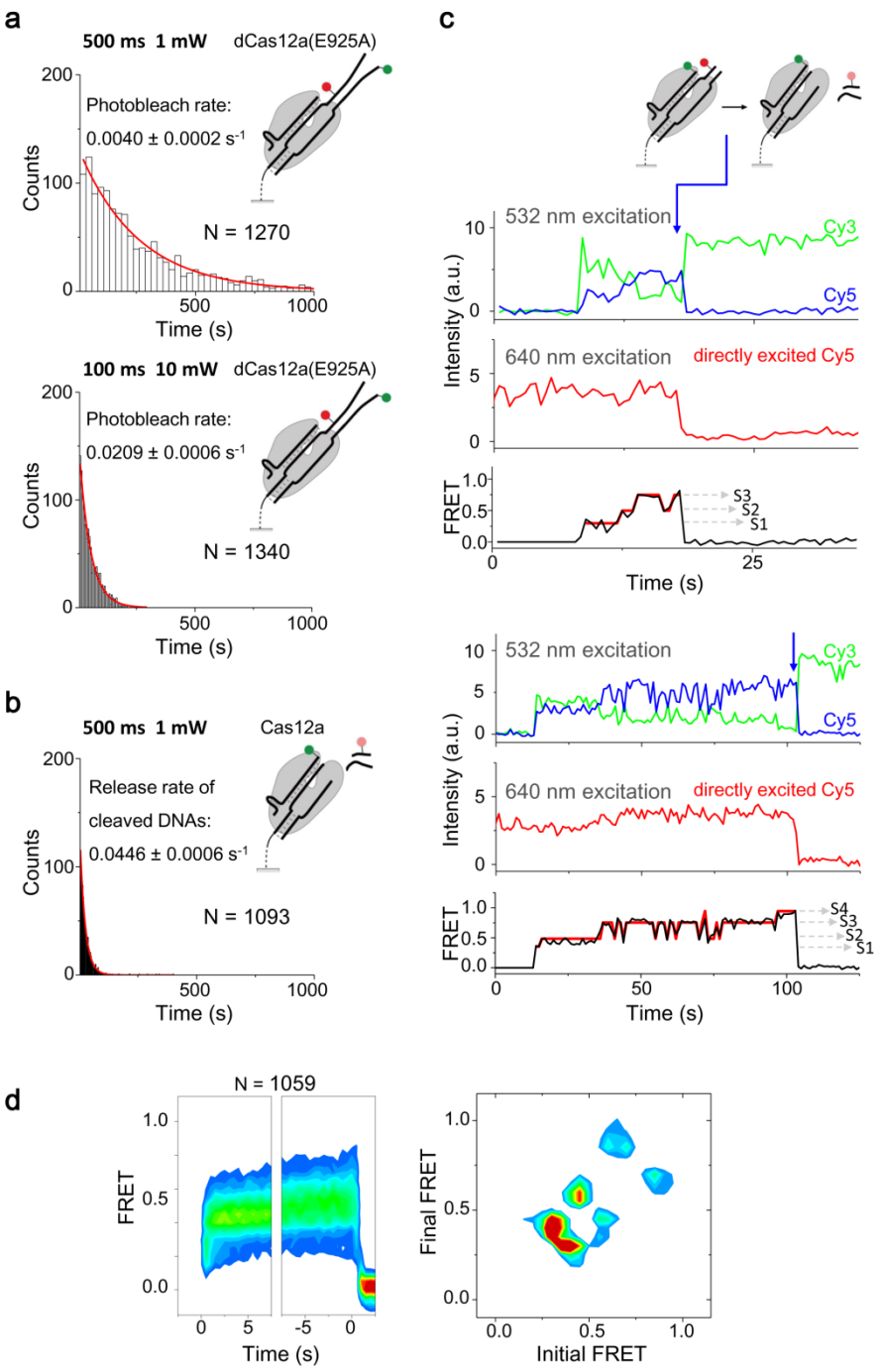

Figure S1. Photobleaching rates, appearance cleavage rates, smFRET trajectories and crRNA-NTS FRET of Cas12a complexes, related to Figure 1. a, Distributions of FRET duration time of labeled dsDNA within dCas12a (E925A) ternary complexes which are unable to cleave DNA. With 500 ms exposure time and 1 mW laser excitation power, FRET disappearance rates caused by Cy3 and Cy5 photobleaching are 0.0036 ± 0.0002 s^{-1} (N = 890) and 0.0052 ± 0.0004 s^{-1} (N = 380), respectively. The overall FRET disappearance rate is 0.0040 ± 0.0002 s^{-1} (top panel). With 100 ms exposure time and 10 mW laser excitation power, FRET disappearance rates caused

by Cy3 and Cy5 photobleaching are 0.020 ± 0.001 s^{-1} (N = 960) and 0.029 ± 0.003 s^{-1} (N = 380), respectively. The overall FRET disappearance rate is 0.021 ± 0.001 s^{-1} (bottom panel). **b**, FRET disappearance rate caused by release of cleaved DNA from Cas12a ternary complexes containing Cy3-labeled crRNA and Cy5-labeled dsDNA using 500 ms exposure time and 1 mW laser excitation power. With these instrumental settings, contributions of photobleaching is < 10%. **c**, Representative smFRET trajectories of DNA cleavage events under alternating-laser excitation of 532 nm and 640 nm lasers, from which disappearance of Cy3 and Cy5 are captured independently. FRET disappearance from either S3 or S4 is accompanied by Cy5 signal disappearance, which indicates that termination of FRET is caused by release of cleaved Cy5-labeled DNA fragment. Such phenomena suggest that both S3 and S4 states are DNA pre-cleavage states. **d**, Time-dependent FRET probability density plot and transition density plot of Cas12a complexes on 23m-dsDNA captured using FRET pairs located on crRNA and NTS. Cy3 is labeled at 3' end of crRNA, Cy5 is labeled at the NTS 30 nt away from the PAM.

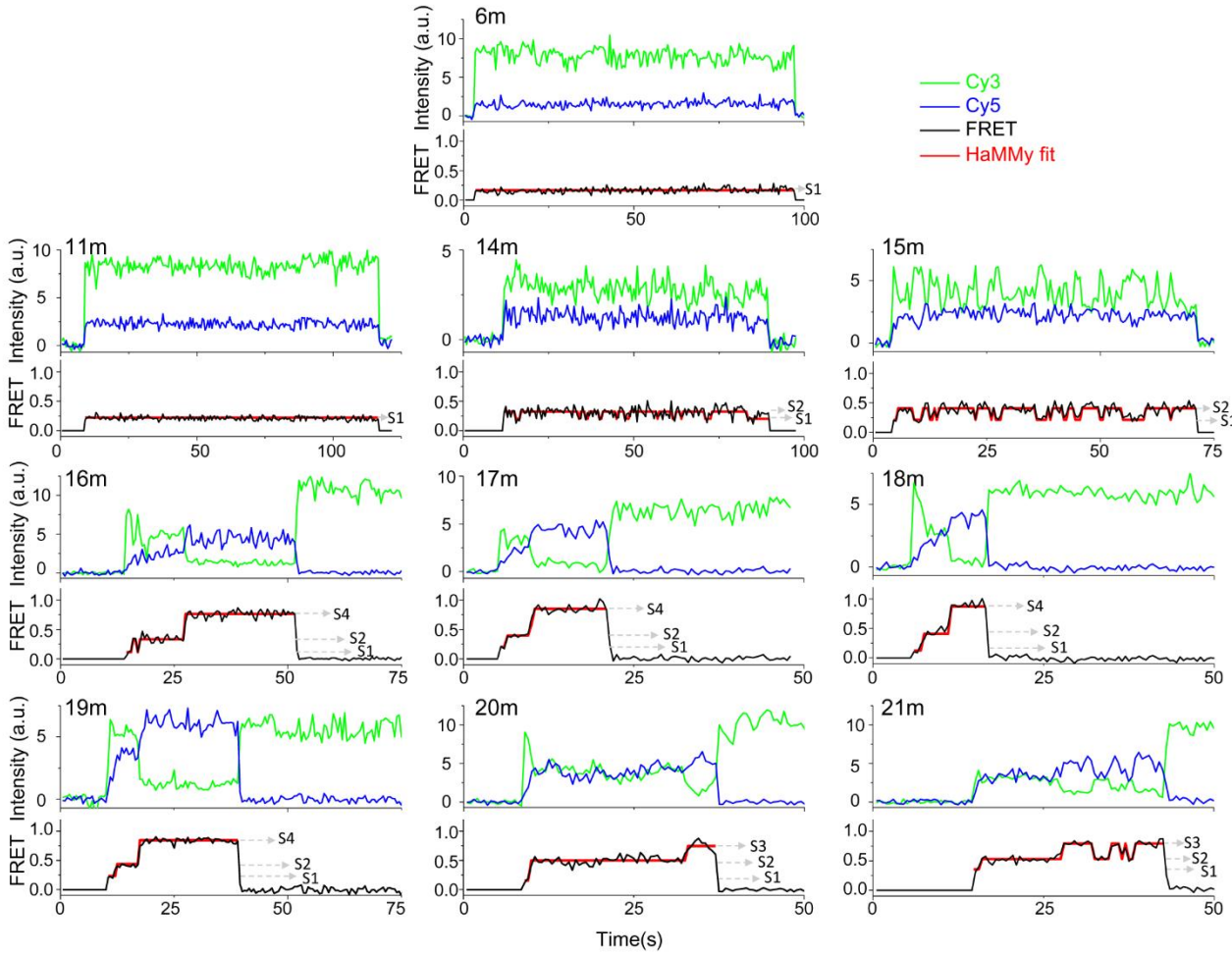

Figure S2. Representative smFRET trajectories of Cas12a ternary complexes on partial cognate dsDNAs, related to Figure 2. Representative smFRET traces of Cas12a complexes on 6m-, 11m-, 14m-, 15m-, 16m-, 17m-, 18m-, 19m-, 20m- and 21m-dsDNAs. Black lines are apparent FRET efficiencies and red lines are hidden Markov modeling of FRET. Under 532 nm excitation, spontaneous appearance of Cy3 and Cy5 (due to FRET) signals represents the formation of Cas12a ternary complex on immobilized dsDNA. Simultaneous disappearance of FRET and Cy3 is caused by dissociation of Cy3-labeled Cas12a/crRNA from immobilized Cy5-labeled DNA, whereas disappearance of FRET accompanied by increasing of Cy3 intensity corresponds to dissociation of the cleaved Cy5-labeled PAM-distal DNA fragment.

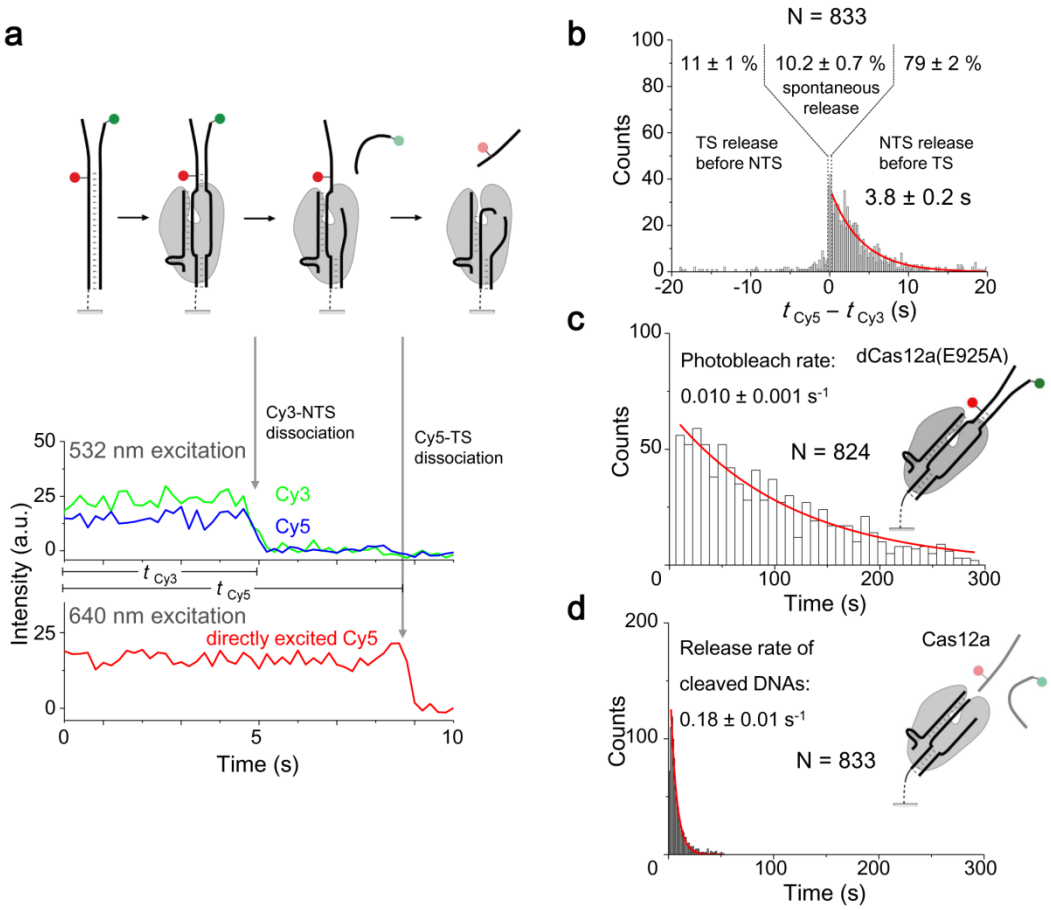

Figure S3. Release of cleaved DNA fragments examined using fluorophore labeled NTS and TS, related to Figure 2. a, smFRET trajectories and cartoons illustrating dissociation of Cy3-labeled NTS and Cy5-labeled TS. Under alternating-laser excitation of 532 nm and 640 nm lasers, disappearance of Cy3 and Cy5 can be captured independently. Times from injecting unlabeled Cas12a/crRNA into flow channels containing immobilized dsDNAs until disappearance of Cy3 and Cy5 are extracted from individual single-molecule trajectories and defined as t_{Cy3} and t_{Cy5}, respectively. **b**, Distribution of t_{Cy5} - t_{Cy3}. 79% ± 2% of events have Cy5-NTS disappear before Cy3-TS, whereas only 11% ± 1% of events have Cy3-TS disappear before Cy5-NTS. Single-exponential fitting shows that, for the majority of molecules, cleaved TS is released 3.8 ± 0.2 s after cleaved NTS. **c**, Photobleaching rate measured using dCas12a. Power of 532 nm and 640 nm lasers are 5 mW and 3 mW, respectively, with 100 ms exposure time. **d**, Apparent release rate of cleaved Cy3-NTS fragments after formation of Cas12a ternary complexes, which is an order of magnitude faster than photobleaching rate.

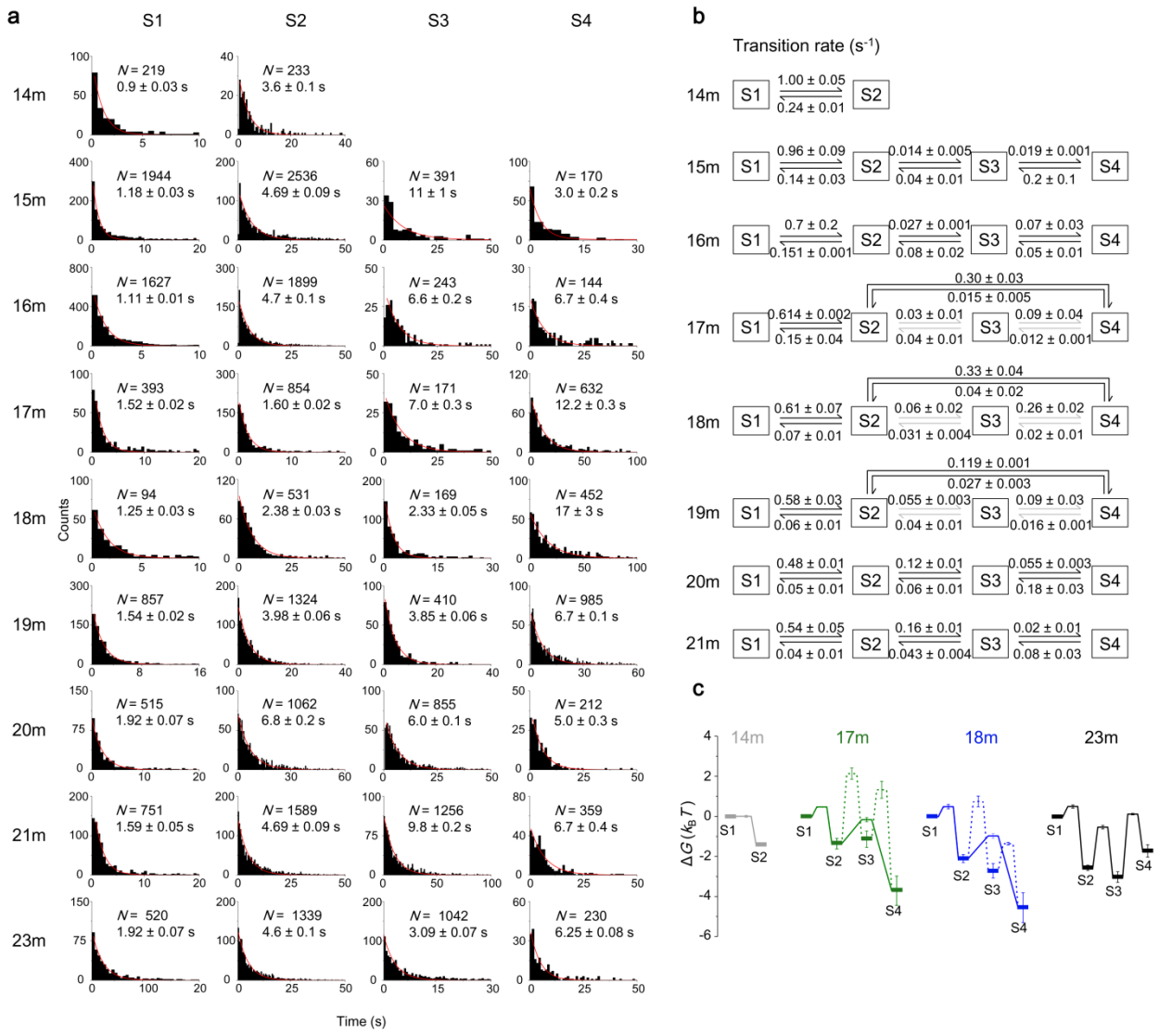

Figure S4. Kinetic schemes and energy landcapes of Cas12a ternary complexes, related to Figure 2. a, Distributions of dwell time extracted from HMM modeling. Average dwell times fitted from single-exponential decay curve and number of events (*N*) from a representative experiment were shown. Three to five repeats were used when calculating transition rates among FRET states shown in b. **b**, Kinetic schemes showing transition pathways and rates among different FRET states. Arrows in black and grey indicate major and minor transition pathways, respectively. **c**, Energy landscapes of Cas12a complexes on 14m-, 17m-, 18m- and 23m-dsDNAs. Bold horizontal lines represent four conformational states captured by smFRET, and thin horizontal lines represent energy barriers along transition pathways. For 17m- and 18m-dsDNA which contains parallel reaction pathways, the major pathway is shown in solid lines and the minor pathway is in dash lines. k_B is Boltzmann constant and T is temperature.

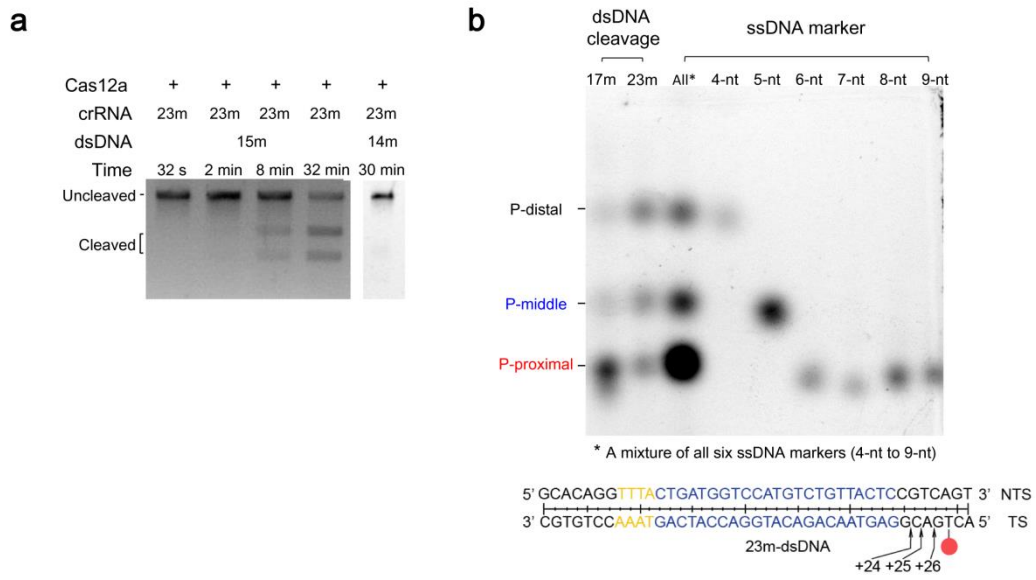

Figure S5. Cleavage of dsDNAs, related to Figure 3 and 4. a, Cleavage of 15m- and 14m-dsDNAs. 15m-dsDNA is cleaved much slower than dsDNA containing more matches between crRNA and dsDNA as shown in Fig. 2c. Prolonged cleavage time (8 min and 32 min) results in detectable dsDNA cleavage. 14m-dsDNA cannot be cleaved within 30 min. **b**, Cleavage sites on target strand (TS) of dsDNA. Cy5 labeled single-stranded DNAs (ssDNAs) of different length were resolved on 20% urea-PAGE gel to illustrate TS cleavage sites as shown in Fig. 3b. The band named 'P-distal' represented a 4-nt-length product, indicating a cleavage site at position + 26 of TS; 'P-middle' product resulted from cleavage at position + 25, and 'P-proximal' originated from cleavage at position about + 24.

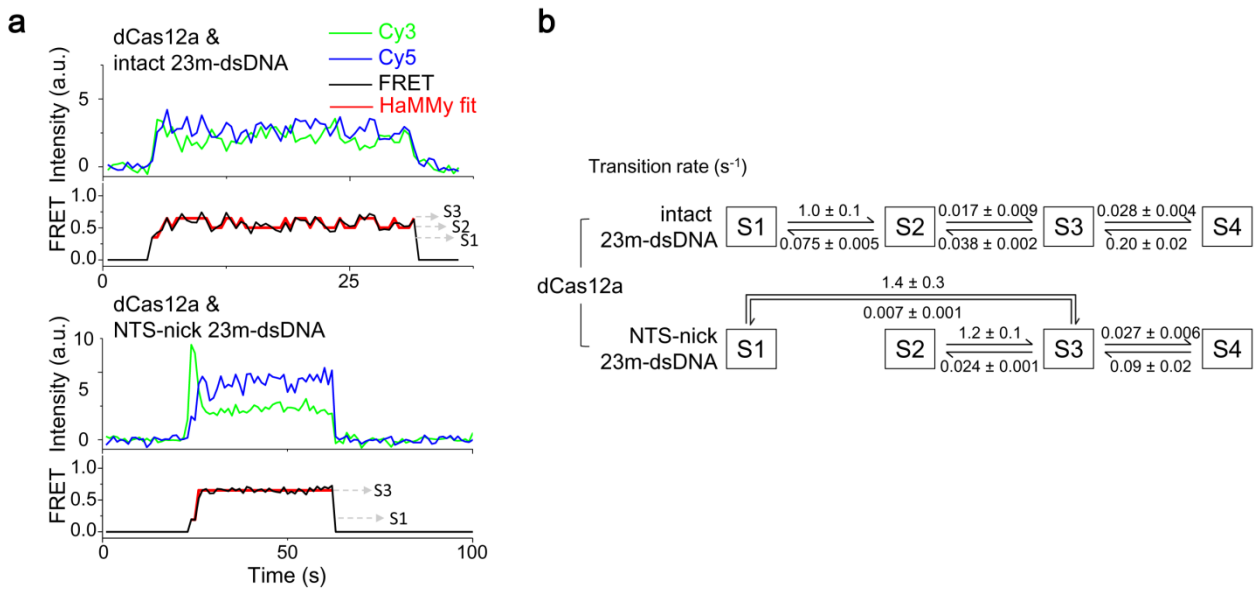

Figure S6. Representative smFRET trajectories and kinetic schemes of dCas12a ternary complexes, related to Figure 5. a, Representative smFRET trajectories of dCas12a complexes on intact and NTS-nick dsDNAs. **b**, Kinetic schemes showing transition pathways and rates of dCas12a complexes on intact and NTS-nick dsDNAs.

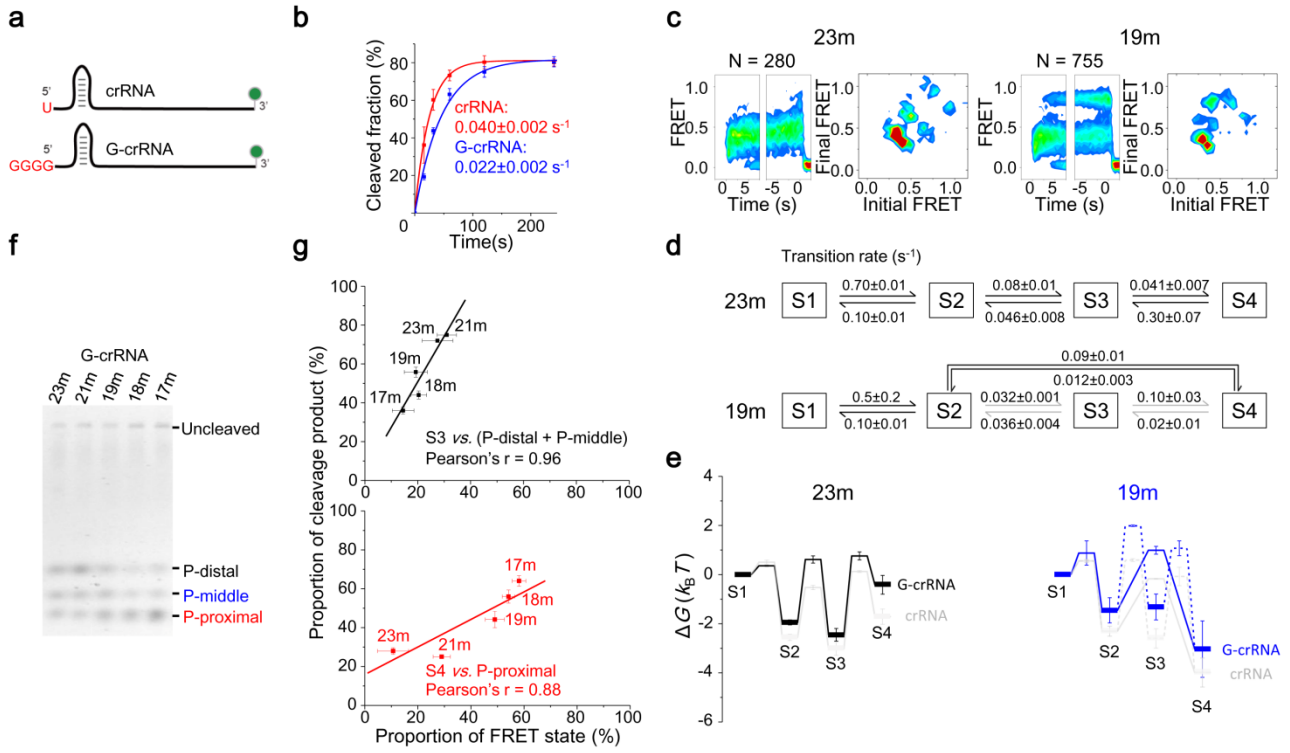

Figure S7. Conformational dynamics and cleavage patterns of Cas12a complexes guided by G-crRNA, related to Figure 2 and 3. a, Cartoon illustrating difference between crRNA and G-crRNA. Four G nucleotides at the 5' end of G-crRNA replace a single U at the 5' end of crRNA used in all other experiments. The other sequences remain the same. **b**, Time-dependent 23m-dsDNA cleavage using crRNA and G-crRNA. **c-e**, Time-dependent FRET probability density plots and transition density plots (**c**), transition pathways (**d**) and energy landscapes (**e**) of Cas12a/G-crRNA complexes on 23m- and 19m-dsDNAs. Energy landscapes of Cas12a/crRNA/dsDNA complexes are shown in grey for comparison. **f**, Cleavage of full and partial cognate dsDNAs labeled at their TS PAM-distal ends. **g,** Linear correlation between proportion of FRET states in the last frame and proportion of cleavage products shown in **f.** They display a strong positive correlation with Pearson's r = 0.88 ~ 0.96.

Table S1. RNA sequences, related to Figure 1, 2, 3, 4 and 5.

Name	Sequence (from 5' to 3') [a]	Related figures
crRNA (Takara) [b]	UAAUUUCUACUAAGUGUAGAUCUGAUGGUCCAUGUCUGUUACUC-NH_2	Figs. 1, 2, 4d, 5 and S7b
23m-crRNA (transcribed *in-vitro*)	*GGUUUCAAAGAUUAAA*UAAUUUCUACUAAGUGUAGAUCUGAUGGUCCAUGUCUGUUACUC	Figs. 3b, 4
14m-crRNA (transcribed *in-vitro*)	*GGUUUCAAAGAUUAAA*UAAUUUCUACUAAGUGUAGAUCUGAUGGUCCAUGUgacaaugag	Figs. 4b and 4c
G-crRNA (transcribed *in-vitro*) [b]	GGGGAAUUUCUACUAAGUGUAGAUCUGAUGGUCCAUGUCUGUUACUC	Fig. S7

[a] Stem-loop sequences are highlighted in grey, spacer sequences are underlined in which mismatches are shown in lower case, transcribed RNA sequences which will be cleaved by Cas12a to generate matured crRNA are italicized (Singh et al., 2018). 14m-crRNA contains 14 matched bases towards 23m-dsDNA at its PAM-proximal end. The other crRNAs are fully matched towards 23m-dsDNA.

[b] crRNA (Takara) and G-crRNA were labeled with Cy3 at their 3' end before used in smFRET experiments.

Table S2. DNA sequences, related to Figure 1, 2, 3, 4 and 5.

Name	Sequence (5' to 3')
biotin handle	CCCTGGTCCGGTGGTCCGCCTGCTGGTCCC-biotin
dsDNA with 6 or 11 mismatched bases at the PAM-proximal end	
PAMprox6mm_NTS	CGGACCACCGGACCAGGGGCACAGGTTTAgactacGTCCATGTCTGTTACTCCGTCAGT
PAMprox6mm_TS	AC T(-Cy5)GACGGAGTAACAGACATGGACgtagtcTAAACCTGTGC
PAMprox11mm_NTS	CGGACCACCGGACCAGGGGCACAGGTTTAgactaccaggtTGTCTGTTACTCCGTCAGT
PAMprox11mm_TS	AC T(-Cy5)GACGGAGTAACAGACAacctggtagtcTAAACCTGTGC
TS labeled full and partial cognate dsDNAs, related to Figs. 1, 2, 3, S5b and S7	
23m-NTS (S)	CGGACCACCGGACCAGGGGCACAGGTTTACTGATGGTCCATGTCTGTTACTCCGTCAGT
23m-TS (S)	ACT(-Cy5)GACGGAGTAACAGACATGGACCATCAGTAAACCTGTGC
21m-NTS (S)	CGGACCACCGGACCAGGGGCACAGGTTTACTGATGGTCCATGTCTGTTACagCGTCAGT
21m-TS (S)	ACT(-Cy5)GACGctGTAACAGACATGGACCATCAGTAAACCTGTGC
20m-NTS (S)	CGGACCACCGGACCAGGGGCACAGGTTTACTGATGGTCCATGTCTGTTAgagCGTCAGT
20m-TS (S)	ACT(-Cy5)GACGctcTAACAGACATGGACCATCAGTAAACCTGTGC
19m-NTS (S)	CGGACCACCGGACCAGGGGCACAGGTTTACTGATGGTCCATGTCTGTTtgagCGTCAGT
19m-TS (S)	ACT(-Cy5)GACGctcaAACAGACATGGACCATCAGTAAACCTGTGC
18m-NTS (S)	CGGACCACCGGACCAGGGGCACAGGTTTACTGATGGTCCATGTCTGTatgagCGTCAGT
18m-TS (S)	ACT(-Cy5)GACGctcatACAGACATGGACCATCAGTAAACCTGTGC
17m-NTS (S)	CGGACCACCGGACCAGGGGCACAGGTTTACTGATGGTCCATGTCTGaatgagCGTCAGT
17m-TS (S)	ACT(-Cy5)GACGctcattCAGACATGGACCATCAGTAAACCTGTGC
16m-NTS (S)	CGGACCACCGGACCAGGGGCACAGGTTTACTGATGGTCCATGTCTcaatgagCGTCAGT
16m-TS (S)	ACT(-Cy5)GACGctcattgAGACATGGACCATCAGTAAACCTGTGC
15m-NTS (S)	CGGACCACCGGACCAGGGGCACAGGTTTACTGATGGTCCATGTCacaatgagCGTCAGT
15m-TS (S)	ACT(-Cy5)GACGctcattgtGACATGGACCATCAGTAAACCTGTGC
14m-NTS (L)	CGGACCACCGGACCAGGGGCACAGGTTTACTGATGGTCCATGTgacaatgagCGTCAGTCGAGGCT CTCGAC
14m-TS (L)	GTCGAGAGCCTCGACT(-Cy5)GACGctcattgtcACATGGACCATCAGTAAACCTGTG
11m-NTS (S)	CGGACCACCGGACCAGGGGCACAGGTTTACTGATGGTCCAacagacaatgagCGTCAGT
11m-TS (S)	ACT(-Cy5)GACGctcattgtctgtTGGACCATCAGTAAACCTGTGC

6m-NTS (S)	CGGACCACCGGACCAGGGGCACAGGTTTACTGATGcaggtacagacaatgagCGTCAGT
6m-TS (S)	ACT(-Cy5)GACGctcattgtctgtacctgCATCAGTAAACCTGTGC
NTS labeled full cognate dsDNAs, related to Fig. S1d and 4c	
23m-NTS (L)	CGGACCACCGGACCAGGGGCACAGGTTTACTGATGGTCCATGTCTGTTACTCCGTCAGT(-Cy5)CGAGGCTCTCGAC
23m-TS (L)	GTCGAGAGCCTCGACTGACGGAGTAACAGACATGGACCATCAGTAAACCTGTG
dsDNA with both NTS and TS labeled, related to Fig. S3	
Cy3-23m-NTS (L)	CGGACCACCGGACCAGGGGCACAGGTTTACTGATGGTCCATGTCTGTTACTCCGAGTCAGCTCCGAGAGCTG(-Cy3)
Cy5-23m-TS (L)	GTCGAGAGCCTCGACT(-Cy5)GACGGAGTAACAGACATGGACCATCAGTAAACCTGTG
Non-specific ssDNA and pre-unwound dsDNA, related to Figs. 4a-b	
14m activator	ctcattgtcACATGGACCATCAGTAAACCTGTG
23m activator	GAGTAACAGACATGGACCATCAGTAAACCTGTG
non-specific ssDNA	(Cy5-)TCTGCGTATTTCTTGAGACGCTGGAGTACAATCGTCTGAGACGCTGGTCAGCTCTCTGA
NTS_23m	(Cy5-)AGTCTCTTGGCACAGGtttaCTGATGGTCCATGTCTGTTACTCcggaattcgagtacaa
TS_23m	(AF488-)ttgtactcgaattccgGAGTAACAGACATGGACCATCAGtaaaCCTGTGCCAAGAGACT
TS_14m_9mm	(AF488-)ttgtactcgaattccgctcattgtcACATGGACCATCAGtaaaCCTGTGCCAAGAGACT
NTS_17m_6mm	(Cy5-)AGTCTCTTGGCACAGGtttaCTGATGGTCCATGTCTGaatgagcggaattcgagtacaa
6m+8mm+9m_NTS	(Cy5-)AGTCTCTTGGCACAGGtttaCTGATGcaggtacaCTGTTACTCcggaattcgagtacaa
6m+17mm_TS	(AF488-)ttgtactcgaattccgctcattgtctgtacctgCATCAGtaaaCCTGTGCCAAGAGACT
6m+8mm+3m+6mm_NTS	(Cy5-)AGTCTCTTGGCACAGGtttaCTGATGcaggtacaCTGaatgagcggaattcgagtacaa
Full and partial cognate dsDNAs containing pre-cleaved NTS (NTS-nick) or pre-cleaved TS (TS-nick), related to Figs. 4c-d and 5	
23m-NTS (L)	CGGACCACCGGACCAGGGGCACAGGTTTACTGATGGTCCATGTCTGTTACTCCGTCAGTCGAGGCTCTCGAC
Cy5-23m-NTS (L)	CGGACCACCGGACCAGGGGCACAGGTTTACTGATGGTCCATGTCTGTTACTCCGTCAGT(-Cy5)CGAGGCTCTCGAC
23m-NTS(A) (L)	CGGACCACCGGACCAGGGGCACAGGTTTACTGATGGTCCATGTCTGT
23m-NTS(B) (L)	ACTCCGTCAGTCGAGGCTCTCGAC

Cy5-23m-TS (L)	GTCGAGAGCCTCGACT(-Cy5)GACGGAGTAACAGACATGGACCATCAGTAAACCTGTG
23m-TS (L)	GTCGAGAGCCTCGACTGACGGAGTAACAGACATGGACCATCAGTAAACCTGTG
23m-TS(A) (L)	GAGTAACAGACATGGACCATCAGTAAACCTGTG
23m-TS(B) (L)	GTCGAGAGCCTCGACTGACG
20m-NTS(A) (L)	CGGACCACCGGACCAGGGGCACAGGTTTACTGATGGTCCATGTCTGT
20m-NTS(B) (L)	AgagCGTCAGTCGAGGCTCTCGAC
Cy5-20m-TS (L)	GTCGAGAGCCTCGACT(-Cy5)GACGctcTAACAGACATGGACCATCAGTAAACCTGTG
18m-NTS(A) (L)	CGGACCACCGGACCAGGGGCACAGGTTTACTGATGGTCCATGTCTGT
18m-NTS(B) (L)	tgagCGTCAGTCGAGGCTCTCGAC
Cy5-18m-TS (L)	GTCGAGAGCCTCGACT(-Cy5)GACGctcatACAGACATGGACCATCAGTAAACCTGTG
17m-NTS(A) (L)	CGGACCACCGGACCAGGGGCACAGGTTTACTGATGGTCCATGTCTGa
17m-NTS(B) (L)	tgagCGTCAGTCGAGGCTCTCGAC
Cy5-17m-TS (L)	GTCGAGAGCCTCGACT(-Cy5)GACGctcattCAGACATGGACCATCAGTAAACCTGTG
14m-NTS(A) (L)	CGGACCACCGGACCAGGGGCACAGGTTTACTGATGGTCCATGTgaca
14m-NTS(B) (L)	tgagCGTCAGTCGAGGCTCTCGAC
Cy5-14m-TS (L)	GTCGAGAGCCTCGACT(-Cy5)GACGctcattgtcACATGGACCATCAGTAAACCTGTG
ssDNA marker, related to Fig. S5b	
9nt marker	AC T(-Cy5)GACGGA
8nt marker	AC T(-Cy5)GACGG
7nt marker	AC T(-Cy5)GACG
6nt marker	AC T(-Cy5)GAC
5nt marker	AC T(-Cy5)GA
4nt marker	AC T(-Cy5)G

'*N*m' stands for that the number of PAM-proximal matched bases is *N* and mismatches are shown in lower case. Internal labeled bases are highlighted in yellow. '(S)' and '(L)' represent two different DNA series used to form dsDNAs with a total length of 59 bp and 72 bp, respectively. 72 bp-length dsDNAs were used to introduce NTS-nicks and TS-nicks. The PAM and target sequence were remained the same within these two series of dsDNAs.

Table S3. Sequence of linearized dsDNA for *in-vitro* cleavage, related to Figs. 2c and S5.

Full cognate sequence (from 5' to 3')
CGCAGAAGTGGTCCTGCAACTTTATCCGCCTCCATCCAGTCTATTAATTGTTGCCGGGAAGCTAGAGTAAG
TAGTTCGCCAGTTAATAGTTTGCGCAACGTTGTTGCCATCGCTACAGGCATCGTGGTGTCACGCTCGTCGT
TTGGTATGGCTTCATTCAGCTCCGGTTCCCAACGATCAAGGCGAGTTACATGATCCCCCATGTTGTGCAAA
AAAGCGGTTAGCTCCTTCGGTCCTCCGATCGTTGTCAGAAGTAAGTTGGCCGCCGTGTTATCACTCATGGT
TATGGCAGCACTACATAATTCTCTTACTGTCATGCCATCCGTAAGATGCTTTTCTGTGACTGGTGAGTACT
CAACCAAGTCATTCTGAGAATAGTGTATGCGGCGACCGAGTTGCTCTTGCCCGGCGTCAATACGGGATAA
TACCGCGCCACATAGCAGAACTTTAAAAGTGCTCATCATTGGAAAACGTTCTTCGGGGCGAAAACTCTCA
AGGATCTTACCGCTGTTGAGATCCAGTTCGATGTAACCCACTCGTGCACCCAACTGATCTTCAGCATCTTT
TACTTTCACCAGCGTTTCTGGGTGAGCAAAAACAGGAAGGCAAAATGCCGCAAAAAAGGGAATAAGGGC
GACACGGAAATGTTGAATACTCATACTCTTCCTTTTTCAATATTATTGAAGCATTTATCAGGGTTATTGTCT
CATGAGCGGATACATATTTGAATGTATTTAGAAAAATAAACAAATAGGGGTTCCGCGCACATTTCCCCGA
AAAGTGCCACCTGACGTCTAAGAAACCATTATTATCATGACATTAACCTATAAAAATAGGCGTATCACGA
GGCCCTTTCGTTGTAAAACGACGGCCAGTCCGTCTCTATCCGGTCTCGATCCGCAGTCTCTTGGCACAGGT
TTACTGATGGTCCATGTCTGTTACTCCGGAATTCGAGTACAAACGTCAGCACGTGTGTGGCGGAGCGAGG
AGCTGCTGTCCCCGTGGGAGCCGGCCTCAGAGGTAGCTCCATGACCCAGACACCAGTGGGGGATGTCAGT
GTTGGGGGAAAGTAGAAGCTTGGACCGTGCGAGTTACTGCCAACCGAGACCCAACCGAGACGGGTCATA
GCTGTTTCCAGTGTGCCGCTTCCTCGCTCACTGACTCGCTGCGCTCGGTCGTTCGGCTGCGGCGAGCGGTA
TCAGCTCACTCAAAGGCGGTAATACGGTTACCCACAGAATCAGGGGATAACGCAGGAAAGAACATGTGA
GCAAAAGGCCAGCAAAAGGCCAGGAACCGTAAAAAGGCCGCGTTGCTGGCGTTTTTCCATAGGCTCCGC
CCCCCTGACGAGCATCACAAAAATCGACGCTCAAGTCAGAGGTGGCGAAACCCGACAGGACTATAAAGA
TACCAGGCGTTTCCCCCTGGAAGCTCCCTCGTGCGCTCTCCTGTTCCGACCCTGCCGCTTACCGGATACCT
GTCCGCCTTTCTCCCTTCGGGAAGCGTGGCGCTTTCTCAATGCTCACGCTGTAGGTATCTCAGTTCGGTGT
AGGTCGTTCGCTCCAAGCTGGGCTGTGTGCACGAACCCCCCGTTCAGCCCGACCGCTGCGCCTTATCCGGT
AACTATCGTCTTGAGTCCAACCCGGTAAGACACGACTTATCGCCACTGGCAGCAGCCACTGGTAACAGGA
TTAGCAGAGCGAGGTATGTAGGCGGTGCTACAGAGTTCTTGAAGTGGTGGCCTAACTACGGCTACACTAG
AAGGACAGTATTTGGTATCTGCGCTCTGCTGAAGCCAGTTACCTTCGGAAAAAGAGTTGGTAGCTCTTGA
TCCGGCAAACAAACCACCGCTGGTAGCGGTGGTTTTTTTGTTTGCAAGCAGCAGATTACGCGCAGAAAAA
AAGGATCTCAAGAAGATCCTTTGATCTTTTCTACGGGGTCTGACGCTCAGTGGAACGAAAACTCACGTTA

AGGGATTTTGGTCATGAGATTATCAAAAAGGATCTTCACCTAGATCCTTTTAAATTAAAAATGAAGTTTTA
AATCAATCTAAAGTATATATGAGTAAACTTGGTCTGACAGTTACCAATGCTTAATCAGTGAGGCACCTAT
CTCAGCGATCTGTCTATTTCGTTCATCCATAGTTGCCTGACTCCCCGTCGTGTAGATAACTACGATACGGG
AGGGCTTACCATCTGGCCCCAGTGCTGCAATAATACCGCGGGACCCACGCTCACCGGCTCCAGATTTATC
AGCAATAAACCAGCC

PAM sequence is highlighted in cyan, and target sequence (23m) is in yellow. A series of DNAs with different number of matched bases at PAM-proximal ends are used and they target sequences are (from 5' to 3'): CTGATGGTCCATGTCTGTTACTC (23m), CTGATGGTCCATGTCTGTTACag (21m), CTGATGGTCCATGTCTGTTtgag (19m), CTGATGGTCCATGTCTGTatgag (18m), CTGATGGTCCATGTCTGaatgag (17m), CTGATGGTCCATGTCTcaatgag (16m), CTGATGGTCCATGTCacaatgag (15m), CTGATGGTCCATGTgacaatgag (14m). Mismatches towards crRNA are shown in lower case.

Transparent Methods

Plasmid construction, protein expression and purification

The LbCas12a expression plasmid constructed on pGEX-6P-1 was a generous gift from Dr. Zhiwei Huang (Dong et al., 2016), which contains an N-terminal GST tag and a precise protease cleavage site (HRV 3C site). Point mutations were introduced by site-directed mutagenesis and confirmed by DNA sequencing.

E. Coli BL21 (DE3) strain was transformed with LbCas12a expression plasmids, and grown in 2YT medium (100 μg/ml ampicillin) at 37 ℃ to an OD_{600} of 0.6 ~ 0.8. Protein expression was induced by the addition of isopropyl β-d-1-thiogalactopyranoside (IPTG) to a final concentration of 0.7 mM with additional culture for 12-16 h at 16 ℃. Cells were collected and resuspended in lysis buffer (50 mM Tris-HCl pH 7.5, 500 mM NaCl, 1 mM $MgCl_2$, 1 mM freshly prepared TCEP) with 1 mM protease-inhibitor PMSF (Sigma). After sonication, cell debris was removed by a centrifugation step at 14,000 rpm for 45 min at 4 ℃. Supernatant was collected and incubated with glutathione sepharose 4B (GS4B) beads (GE Healthcare) at 4 ℃ for 30 min. Protein was then eluted by GSH elution buffer (50 mM Tris-HCl pH 7.5, 500 mM NaCl, 1 mM $MgCl_2$, 1 mM TCEP, 20 mM GSH), collected, incubated overnight (16 h) with HRV 3C protease (protein : protease =25 : 1) to remove GST tag.

Cation exchange was used for further purification. Firstly, adjust the sodium concentration to 125 mM and pH to 6.0. LbCas12a protein was purified by Source S (GE Healthcare) column using buffer A (50 mM MES pH 6.0, 150 mM NaCl, 1 mM TCEP) and buffer B (50 mM MES pH 6.0, 1 M NaCl, 1 mM TCEP). The integrity and purity of protein were verified by SDS-PAGE electrophoresis. Protein was concentrated in lysis buffer, flash-frozen in aliquots, and stored at -80 ℃.

in-vitro RNA transcription and purification

crRNAs without chemical modifications were transcribed *in vitro*. Template dsDNA containing a T7 promoter followed by a sequence corresponding to crRNA transcript was prepared through a PCR reaction with two single-stranded DNAs (Sangon Biotech, Shanghai, China). dsDNAs with correct length were recovered from agarose gels. The HiScribe T7 kit (NEB) was used for *in-vitro* transcription. crRNAs were purified by gel electrophoresis on a 10% denaturing (8 M urea) polyacrylamide gel. Gel bands containing crRNAs were excised and soaked in soaking buffer (1

mM EDTA, 100 mM NaOAc pH 5.2) at 50 ℃ for 2 h. crRNAs were precipitated by ethanol precipitation, resuspended in nuclease-free water (Life tech), and stored at -80 ℃.

To avoid RNA degradation, nuclease-free water was used in all RNA-related experiments. Before used in cleavage assays, crRNAs were annealed by a pre-heat at 95 ℃ for 10 min and a subsequent gradual temperature decrease (-5 ℃/min) to room temperature.

Amine-derivated DNA/RNA labeling

Amine-derivated DNA (Sangon Biotech, Shanghai, China) or crRNA (Takara) was dissolved to 0.5~1 mM in 10 mM $NaHCO_3$ (Sigma) buffer. Cy3-NHS or Cy5-NHS (Lumiprobe) was then added to a final concentration of 10 mM. The labeling mixture was incubated in the dark at 25 ℃ for at least 2 h. Labeled nucleic acids were purified via ethanol precipitation for three times. Pellet was dried in the air and dissolved in nuclease-free water (Life tech). Concentrations of nucleic acids, Cy3 and Cy5 were estimated by A_{260}, A_{549} and A_{649}, respectively.

3' labeling of RNA

RNA 3' labeling procedure was modified from a previous method (Odom et al., 1980), based on selective periodate oxidation of RNA at its 3' end and reaction of the oxidized product with hydrazide. Detailed procedure was describe before. (Yang et al., 2018)

In-vitro cleavage assay

Cas12a and annealed-crRNAs were pre-incubated to form binary complexes at 37 ℃ for 10 min and applied to target dsDNAs in cleavage buffer (50 mM KOAc, 20 mM Tris-OAc pH 7.9, 10 mM $MgOAc_2$) at 25 ℃. The reactions were stopped by the addition of 6× DNA loading buffer (NEB) or 2× formamide loading. Standard errors of the mean were calculated from three or more replicates.

For non-specific single-stranded DNA (ssDNA) cleavage in Fig. 4a, 375 nM Cas12a, 250 nM crRNA and 250 nM ssDNA activator were incubated at 37 ℃ for 10 min before applied to non-specific ssDNA at 25 ℃ for 20 min. For dsDNA cleavage assays in Figs. 2c and S5a, 75 nM Cas12a and 50 nM crRNA were applied to dsDNA. In Fig. 4b, 375 nM Cas12a and 250 nM crRNA were used to cleave 20 nM labeled dsDNAs for 20 min. In Figs. 3b, 4c, S5b and S7f, 150 nM Cas12a and 100 nM crRNA were used. Uncleaved and cleaved bands of unlabeled linearlized

dsDNA target were separated by 2% agarose gel. Labeled short dsDNAs were resolved on denaturing PAGE gels.

smFRET experiment

All smFRET experiments were performed at 25 ℃ using a home-built objective-type TIRF microscope in cleavage buffer with an oxygen scavenging system containing 3 mg/mL glucose, 100 μg/mL glucose oxidase (Sigma-Aldrich), 40 μg/mL catalase (Roche), 1 mM cyclooctatetraene (COT, Sigma-Aldrich), 1 mM 4-nitrobenzylalcohol (NBA, Sigma-Aldrich), 1.5 mM 6-hydroxy-2,5,7,8-tetramethyl-chromane-2-carboxylic acid (Trolox, Sigma-Aldrich). Details of the TIRF microscope were described before. (Peng et al., 2017)

Cas12a or dCas12a was pre-incubated with crRNAs at ~1 μM at 37 ℃ for 10 min and then diluted to working concentrations. Target dsDNAs were firstly immobilized on the cover slide via biotin-streptavidin interaction. Laser powers were adjusted to prolong the time window of signal detection. Fluorescent signals were recorded at 500 ms/frame and started several seconds before flowing binary complexes. A mixture of 2.5 nM labeled crRNA and 15 nM Cas12a or dCas12a was used to capture dynamics of ternary complexes, whereas a mixture of 1 μM crRNA and 1 μM Cas12a was used to examine release of labeled non-target and target strands.

smFRET data analysis

Collected movies were analyzed by a custom-made software program. Fluorescence spots were fitted by a 2-D Gaussian function within a 9-pixel by 9-pixel area, matching the donor and acceptor spots using a variant of the Hough transform (Illingworth and Kittler, 1987). The background subtracted total volume of the 2-D Gaussian peak was used as raw fluorescence intensity *I*.

FRET traces displayed anti-correlation behaviors between donor and acceptor fluorescent signals were picked and further analyzed by a Hidden Markov Model based software (McKinney et al., 2006). Four FRET states from low to high FRET values were identified as S1 - S4. Transition rates (k) among FRET states were extracted from their dwell times. Relative free energies were calculated through

$$\Delta G_b - \Delta G_a = -k_B T \cdot \ln\left(\frac{k_{a\to b}}{k_{b\to a}}\right)$$

in which k_B is the Boltzmann constant, T is the temperature, $k_{a\to b}$ and $k_{b\to a}$ are transition rates from state a to b and from state b to a, respectively. S1 was set as the ground state $(\Delta G_1 = 0)$. The energy barrier from state a to b was calculated as $-k_B T \ln(k_{a\to b})$.

Supplemental Reference

Singh, D., Mallon, J., Poddar, A., Wang, Y., Tippana, R., Yang, O., Bailey, S., and Ha, T. (2018). Real-time observation of DNA target interrogation and product release by the RNA-guided endonuclease CRISPR Cpf1 (Cas12a). *Proceedings of the National Academy of Sciences of the United States of America* **115,** 5444-5449. doi:10.1073/pnas.1718686115